Feel free to get in contact: geo.david.fernandez@gmail.com

Jbel Amsittene Anticline is a fault propagation fold verging north.

Evidence suggests Upper Jurassic-Lower Cretaceous NNW-SSE to NNE-SSW shortening.

Evolution favours a "tectonics-drives-salt" over a "salt-drives-tectonics" models

Evolution points to factors other than small-cell mantle convection

Anticline growth by shortening during crustal exhumation of the Moroccan Atlantic margin

Fernández-Blanco, D.[1], Gouiza, M.[2], Charton, R.[1,5], Kluge, C.[1], Klaver, J.[3], Brautigam, K.[4] and Bertotti, G.[1,5]

[1] TU Delft University, Faculty of Civil Engineering and Geosciences, Delft, Netherlands - corresponding author: geo.david.fernandez@gmail.com
[2] University of Leeds, School of Earth and Environment, Leeds, England, UK
[3] RWTH Aachen University, Structural Geology, Tectonics and Geomechanics, Aachen, Germany
[4] Vrije Universiteit Amsterdam, Tectonics and Structural Geology Department, Amsterdam, Netherlands
[5] North Africa Research Group (NARG)

Abstract

It is unclear how the crustal-scale erosional exhumation of continental domains of the Moroccan Atlantic margin and the excessive subsidence of its rifted domains affected the Late Jurassic-Early Cretaceous post-rift evolution of the margin. To constrain the km-scale exhumation, we study the structural evolution of the Jbel Amsittene. This anticline is located on the coastal plain of the Moroccan Atlantic margin, and is classically considered to have been developed initially by halokinesis in the Late Cretaceous and by contraction during the Neogene. Our structural analysis indicates that the anticline is a fault-propagation fold verging north with Triassic salts at its core and formed by shortening shortly after continental breakup of the Central Atlantic. The anticline grew by NNW-SSE to NNE-SSW contraction, as shown by syn-tectonic wedges, regional kinematic indicators and synsedimentary structures in Upper Jurassic to Lower Cretaceous rocks. It grew further and tightened during the Cenozoic, presumably in relation to the Atlas/Alpine contraction. Our data and interpretation suggest that "tectonic-drives-salt" in the anticline early evolution, which is coeval with the growth of other anticlines along the Moroccan Atlantic margin and widespread km-scale exhumation farther onshore. Anticline growth due to shortening argues for intraplate far-field stresses potentially linked to the geodynamic evolution of the African, American and European plates.

1 Introduction

The evolution of the Atlantic rifted margin in Morocco (Fig. 1) is marked by a period of atypically excessive subsidence during the Late Jurassic-Early Cretaceous (Gouiza, 2011; Bertotti and Gouiza, 2012). This early post-rift subsidence affected the distal deep basins, the continental shelf and the proximal coastal basins of the Atlantic margin, and was coeval with km-scale erosional exhumation of large continental domains to the east (Ghorbal et al., 2008; Ghorbal, 2009; Saddiqi et al., 2009; Oukassou et al., 2013; Leprêtre et al., 2015a; Gouiza et al., 2017). The underlying process behind this exhumation is still unclear, for it took place ~30 to ~50 My after lithospheric breakup between Morocco and Nova Scotia (Klitgord and Schouten 1986; Sahabi et al. 2004) but prior to the Atlas/Alpine shortening that raised the Atlas and the Rif mountain belts (Frizon de Lamotte et al. 1991, 2008; Laville and Piqué 1992).

Similarly to other passive continental margins where comparable movements were documented in their hinterlands (Japsen and Chalmers, 2000; Japsen et al., 2006, 2009; Peulvast et al., 2008; Bonow et al., 2009), the anomalous vertical movements in Morocco are likely to be driven by tectonic processes. Mechanisms proposed for the Central Atlantic include long wavelength mantle processes (e.g., dynamic topography; e.g., Hoggard et al., 2016; Müller et al., 2018), surface processes (e.g., climate driven enhanced erosion; e.g., Westaway et al., 2009), regional tectonics (e.g., rift uplifted shoulder; e.g., Ruiz et al., 2011) and horizontal far-field stresses linked to rifting onset or mid-oceanic ridge spreading (e.g., Bertotti and Gouiza, 2012; Japsen et al., 2012; Green et al., 2018). Mantle processes alone, such as small-scale convection cells at the base of the mantle lithosphere, cannot explain the crustal km-scale exhumation during the early post-rift (Gouiza, 2011). In this frame, attempts to link the Late Jurassic-Early Cretaceous exhumation in the east to the coeval subsidence in the west have overlooked the existence of contemporaneous NE-SW to NNE-SSW crustal shortening that might have driven both upward and downward vertical movements along the margin (Gouiza, 2011; Bertotti and Gouiza, 2012).

The Essaouira-Agadir Basin is located on the coastal plain of the Atlantic rifted margin of Morocco, bounded to the E and NE by the Palaeozoic basement highs of the Massif Ancien of Marrakech and the

Jebilets, respectively (Fig. 1). These massifs have experienced substantial exhumation in the early post-rift history (Middle-Late Jurassic to Early Cretaceous; e.g., Ghorbal et al., 2008; Ghorbal, 2009), while the Essaouira-Agadir Basin records clastic input in the Middle Jurassic and Early Cretaceous (Duval-Arnould, 2019; Luber et al., 2019). The Essaouira-Agadir Basin is thus an ideal location to investigate the tectonic processes responsible for the km-scale vertical movements (Fig. 1B). Most of the compressional structures observed in the Essaouira-Agadir Basin are attributed to Alpine shortening events leading to the uplift of the Atlas Belt (Hafid et al., 2006; Hafid, 2000; Ellouz et al., 2003). Thickness changes observed in Upper Jurassic to Upper Cretaceous rocks are interpreted as resulting from synsedimentary halokinesis (Hafid et al., 2006; Hafid, 2000). However, other studies show that numerous contractional structures developed during the Late Jurassic-Early Cretaceous in the western High Atlas and surroundings (Gouiza, 2011; Bertotti and Gouiza, 2012; Benvenuti et al., 2017).

The Jbel Amsittene Anticline is located in the central western part of the Essaouira-Agadir Basin and is one of several comparable structures within the western High Atlas basins thought to be formed by salt diapirism from the Late Cretaceous onwards (Piqué et al., 1998; Hafid, 2000; Le Roy and Piqué, 2001). In this work, we carry out a structural analysis of the Jbel Amsittene Anticline (Figs. 1B & 2), based on field observations in the Jurassic and Cretaceous rocks and structural modeling. We present new evidence to discuss the tectonics of the formation of the Jbel Amsittene Anticline and its relationship with the growth of other structures in the context of regional vertical movements in the Maroccan rifted margin of the Central Atlantic.

Figure 1. Maps of tectonic provinces and geology. (A) *Regional map of Morocco showing the major tectono-stratigraphic provinces and basins of coastal Western Morocco (simplified from the geological map of Morocco; Hollard et al. 1985). With indication of the location of Panel B.* ***(B)*** *Geological map of the western High Atlas and Essaouira-Agadir Basin showing the main Triassic-Liassic rift-related structures near the Amsittene Anticline (Hollard et al. 1985; Le Roy and Piqué 2001).*

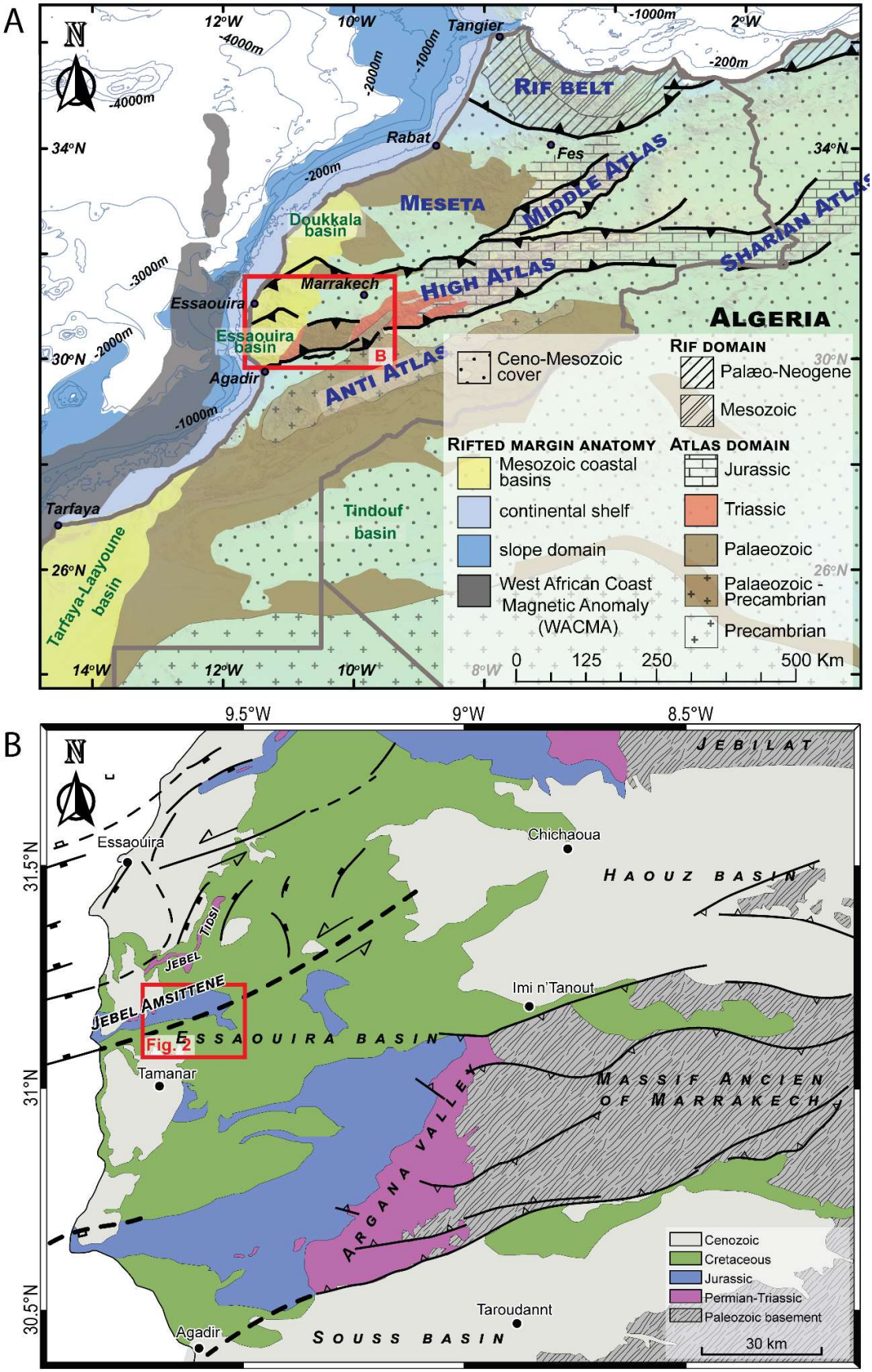
A
N
12°W
10°W
2°W
-4000m
-2000m
-1000m
-200m
Tangier
Rabat
Fes
34°N
30°N
26°N
14°W
Rif belt
Meseta
Middle Atlas
Sharian Atlas
High Atlas
Anti Atlas
Doukkala basin
Essaouira basin
Tindouf basin
Tarfaya-Laayoune basin
Marrakech
Essaouira
Agadir
Tarfaya
B
Algeria
Ceno-Mesozoic cover
Rif domain
Palæo-Neogene
Mesozoic
Rifted margin anatomy
Mesozoic coastal basins
continental shelf
slope domain
West African Coast Magnetic Anomaly (WACMA)
Atlas domain
Jurassic
Triassic
Palaeozoic
Palaeozoic - Precambrian
Precambrian
0 125 250 500 Km
B
9.5°W
9°W
8.5°W
31.5°N
31°N
30.5°N
Essaouira
Chichaoua
Jebilat
Haouz basin
Jebel Tidsi
Jebel Amsittene
Fig. 2
Essaouira basin
Imi n'Tanout
Tamanar
Massif Ancien of Marrakech
Argana valley
Taroudannt
Agadir
Souss basin
Cenozoic
Cretaceous
Jurassic
Permian-Triassic
Paleozoic basement
30 km

2 Geological background

The Essaouira-Agadir Basin forms the western termination of the Moroccan High Atlas (Fig. 1). The basin evolved as part of the Atlantic rift during Triassic to Early Jurassic times and as a proximal shallow-water platform of the rifted Atlantic margin since the Middle Jurassic (e.g., Hafid, 2000). Later convergence between Africa and Iberia/Europe since Late Cretaceous caused N-S to NNW-SSE regional shortening that inverted the Atlas rift, including the Essaouira-Agadir Basin, and built-up the Atlas Mountains (e.g., Hafid et al., 2006; Hafid, 2000; Piqué et al., 2002; Lanari et al., 2020a, 2020b). It is bounded to the south by lithospheric-scale faults, which continue along-strike of the High Atlas belt, and is marked with transpressional and transtensional reactivations since the continental break-up (Ellero et al., 2020).

The Essaouira-Agadir Basin is composed of grabens and half-grabens bounded by N-S to NNE-SSW normal faults and E-W transform faults (Hafid et al., 2006; Hafid, 2000). These extensional rift structures are filled by terrigenous red beds of Triassic age with widespread intercalations of basalt flows, unconformably overlain by an early Lower Jurassic evaporitic sag basin (Hafid et al., 2006). An early Pliensbachian unconformity, which is commonly considered to be the breakup unconformity, seals syn-rift sequences and structures (Medina, 1995). Following continental breakup in the Central Atlantic, sedimentation became mostly marine in the Essaouira-Agadir Basin, leading to accumulation of a thick carbonate platform in the Middle Jurassic to Lower Cretaceous (increasing westwards from 0.5 km to 2 km; e.g., Zühlke et al., 2004), with sandstone and shale interbeds, followed by the deposition of Upper Cretaceous to Neogene shale-dominated series, with intercalations of limestone beds (Hafid, 2000). Shortening in the Atlas domain initiated in the Late Cretaceous, leading to the formation of the Atlas fold-and-thrust belt (Frizon de Lamotte et al., 2000; Piqué et al., 2002; Teixell et al., 2003), and is believed to have triggered the formation of salt-cored anticlines in the Essaouira-Agadir Basin, with minor inversion of Triassic normal faults (Hafid et al., 2006).

Other major tectonic events affected the Moroccan margin after the opening of the Central Atlantic Ocean in addition to the inversion and uplift of the Atlas belt (e.g. Teixell et al., 2003). Low-temperature

thermochronology documents km-scale exhumation that affected most of the Precambrian-Palaeozoic domains exposed to the east of the Atlantic margin (i.e. Meseta plateau, Jebilet, Massif Ancien of Marrakech, Anti-Atlas belt) during Late Jurassic-Early Cretaceous times (Ghorbal et al., 2008; Ghorbal, 2009; Saddiqi et al., 2009; Ruiz et al., 2011; Oukassou et al., 2013; Sehrt, 2014). The Palaeozoic basement highs bounding the Essaouira-Agadir Basin, the Massif Ancien of Marrakech to the east, and the Jebilet to the northeast, experienced km-scale exhumation during the Late Jurassic-Early Cretaceous (Ghorbal, 2009; Saddiqi et al., 2009). Coeval exhumation events are also documented along the margin in the Meseta plateau to the north (Ghorbal, 2009; Saddiqi et al., 2009) and in the Anti-Atlas to the south (Malusà et al., 2007; Ruiz et al., 2011; Oukassou et al., 2013; Sehrt, 2014; Gouiza et al., 2017; Charton et al., 2018). This regional exhumation seems to have occurred during the post-rift stage of the Central Atlantic Ocean, i.e. ~30 to ~50 Myr after lithospheric breakup between Morocco and Nova Scotia (Klitgord and Schouten, 1986; Sahabi et al., 2004), and thus, before the Atlas/Alpine contraction that gave rise to the Atlas and the Rif mountain belts (Frizon de Lamotte et al., 1991, 2008; Laville and Piqué, 1992) and related km-scale exhumation (Lanari et al., 2020b).

Jbel Amsittene is a well-exposed salt-cored anticline that strikes ENE-WSW (Fig. 2A). It is located on the coastal plain of the W Moroccan Atlantic margin, in the northwest of the Essaouira-Agadir Basin between the cities of Essaouira to the north and Agadir to the south (Fig. 1). The Jbel Amsittene Anticline has a limited extent to the west where offshore seismic data shows no folding ~10 km off the present coastline (Hafid et al., 2006).

The stratigraphy of Jbel Amssittene used in this study is based on Duffaud et al. (1966), Jaïdi et al, (1970) and Zühlke et al. (2004). The stratigraphic column shown in Fig. 2B is taken from the 1:100000 geologic map of the study area (Jaïdi et al., 1970), and shows an almost-continuous series of Upper Triassic to Lower Cretaceous rocks unconformably covered, near the coast, by Quaternary sediments. The oldest formation, exposed in the core of the anticline, comprises Upper Triassic (T) terrigenous sandstones and evaporites. An erosional event, marked by a stratigraphic gap, occurred before Early Jurassic (J0-J1) open-

marine deposition. A gradual transition from floodplain to inner shelf environment during the Middle Jurassic (J2-J3; e.g., Duval-Arnould, 2019), resulted in a sedimentary change from predominantly siliciclastic sand-dominated units to shallow marine carbonates. The Upper Jurassic (J4-J5) sediments are mainly shallow marine carbonates of inner shelf to lagoonal environment, although there are some sandstones and clastic interbeds (Ouajhain et al., 2011). An environmental change from inner (J/C-C1-C2) to outer shelf occurred by the end of the Early Cretaceous (C3). Quaternary terrestrial colluviums and coastal deposits overlie the Mesozoic rocks (Fig. 2).

Figure 2. Geology and chronostratigraphy in the Jbel Amsittene Anticline. ***(A)*** *Geological map of the Jbel Amsittene Anticline, showing the location of the main observations in the field (yellow stars) and cross-sections that have been used to constrain the geological evolution of the area. Outcrops and outcrop numbers are shown as Oc.#.* ***(B)*** *Simplified chronostratigraphic and environmental column of the Jbel Amsittene area. Based on Hafid (2000), the geological map of Tamanar from the Moroccan Geological Survey and Zühlke et al. (2004).*

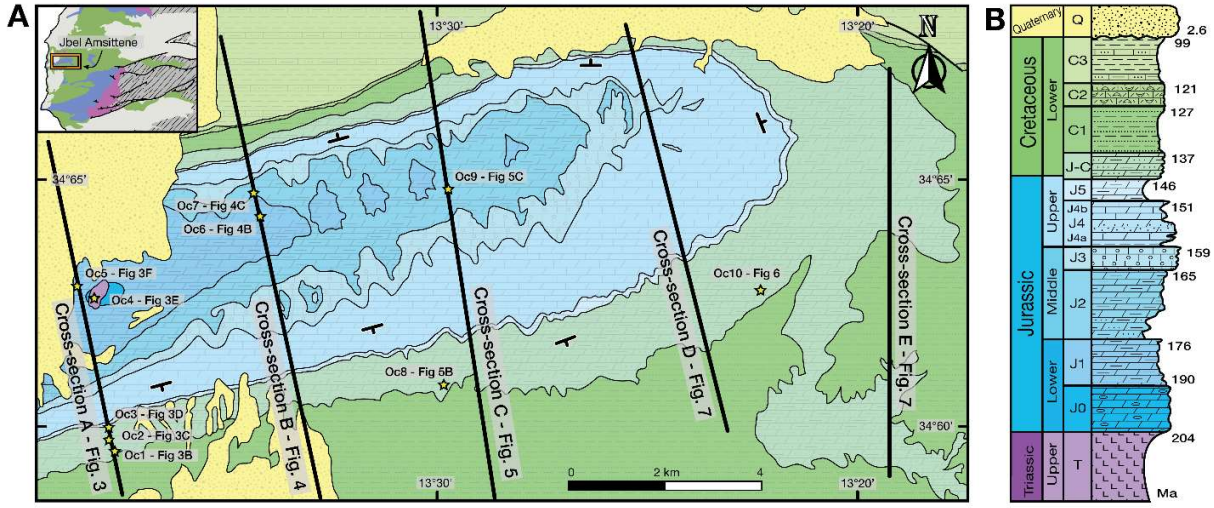

3 Jbel Amsittene Anticline geological cross-sections and field observations

We performed detailed structural fieldwork to understand the tectonic history of the Jbel Amsittene Anticline. Whenever possible, we differentiated between two deformational events; (i) deformation related to Late Jurassic - Early Cretaceous structures involving soft sediment deposition, as a means to assess the stress field during the early post-rift of the Central Atlantic, and (ii) deformation related to (presumably-Cenozoic) Alpine events. We show relevant and representative outcrops (Fig. 2A) that summarize the main structural observations along three cross-sections. We provide uninterpreted pictures of these outcrops and complementary pictures in the Supplementary Material.

The studied geological cross sections are roughly 4 km apart transecting the anticline across its axis, NNW-SSE, and were constrained by bed measurements and field observations. Cross-section A (Fig. 3) is parallel to a road-cut for most of its length, which results in the best rock exposures in the area. Jurassic and Cretaceous rocks outcrop in the south and central parts of the section and are covered by Quaternary deposits in the northern region. Cross-section B (Fig. 4) is located ~4 km east of cross-section A and parallel to it. Cross-section B has sectors with poor accessibility or covered by vegetation and a small number of well-preserved outcrops. Cross-section C (Fig. 5) is ~4 km east of cross-section B, and parallel to the previous sections. We further detail two additional cross-sections and an outcrop farther east. Finally, we describe and recapitulate information relevant for the discussion in the form of along-strike and across-strike lateral variations, syn-sedimentary deformation, and a 3D thickness model.

3.1 Western section: Cross-section A

The lower Lower Cretaceous (C1) to lower Middle Jurassic (J2) limestone, marl, and sandstone layers dip south in most of the southern flank and change from horizontal to steeply north-dipping where the topography is the highest. North of the topographic high, layers dip south again and finally outcrop as overturned, prior to being covered by Quaternary deposits in the northernmost area of the section.

Quaternary rocks prevent an unambiguous thickness comparison between the older units on both sides of the anticline. Those that could be compared showed no changes in thicknesses. The transition from horizontal to overturned layers is observed in the oldest Jurassic limestones and shales exposed in this section (lowermost Jurassic, J1). The dip of the stratigraphic layers indicates a northward verging anticline with a tête-plongeante (plunging head) shape (sensu Seguret, 1972) in its central-northern sectors.

Lower Cretaceous marls and carbonates dip gently to the south (10˚-20˚) in the southernmost part of the southern flank ("a" in Fig. 3A), and become steeper towards the north, reaching dips of ~80˚ at the highest point of the topography. Changes in dip are not constant and north dipping layers outcrop in the central sector of the southern flank (Fig. 3A), within the middle and lower Upper Jurassic shales, marls and limestones (J4). Moving northwards, the dip of the layers locally changes in relation to secondary N-verging folds tens of meters in size. Three conjugate fault sets outcrop in a local topographic flat (Fig. 3A), in the uppermost Upper Jurassic-lowermost Lower Cretaceous (J-C) limestones. We identify conjugate sets as faults with the same kinematics, coherent dip and dip angle (between ~45-60°), and independently-measured striae on both fault planes located at ~90° from the fault planes intersection, and derive the orientation of the stress ellipsoid from the striations of conjugate faults (Fig. 3B). We show one of them in Oc1 (Fig. 3B). The regional bedding dips gently to the SSE, and the three conjugate fault sets show clear striations of sub-horizontal to gently S directions (from 216/04 to 171/20). The fault planes and associated striations are indicative of N-S to NNE-SSW maximum horizontal stresses, both for limestones rotated with respect to the regional bedding (post-tilted) and non rotated (pre-tilted). From this outcrop northwards, bed dips start to increase and reach values up to ~55˚ toward the south ("b"; Fig. 3A). Less than 50 m before the exposure of the lower Lower Cretaceous limestones and marls (C1), a N-S-striking sub-vertical clastic dyke of marine clastics cuts S-dipping strata (Oc2; Fig. 3C). A few meters northwards, a syn-sedimentary N-verging ramp fold indicates soft sediment deformation (Oc3; Fig. 3D). Whereas the conjugate fault set in Oc.1 (Fig. 3B) suggests no deformation took place before deposition of uppermost Upper Jurassic –

lowermost Lower Cretaceous unit (J-C), the latter two syn-sedimentary structures (Oc2; Oc3, Figs. 3C, 3D) indicate NNW-SSE shortening during its deposition.

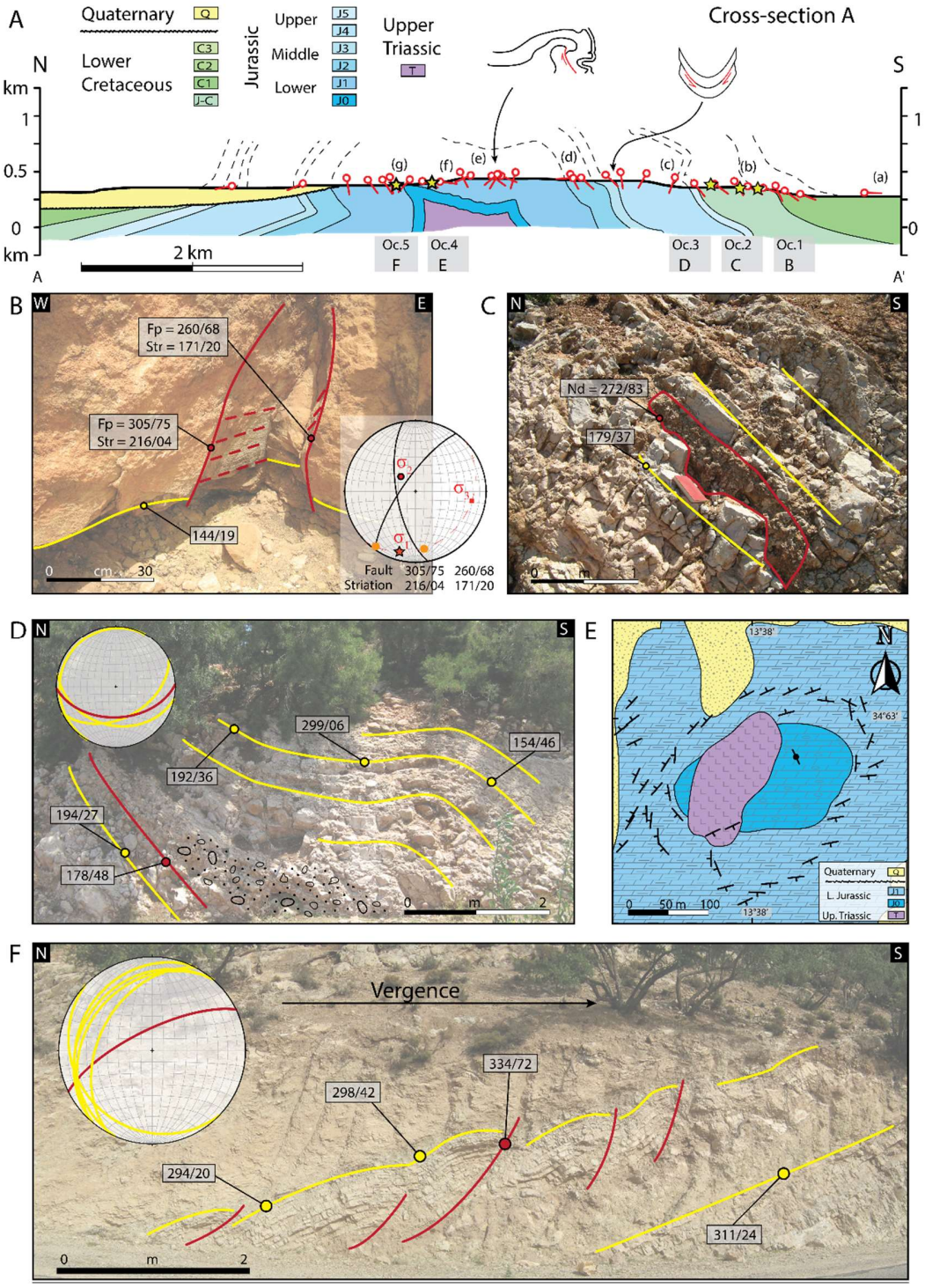

Figure 3. Western section and main outcrops. ***(A)*** *Cross-section A.* ***(B)*** *Outcrop 1. Limestones with regional bedding shown in yellow and faults and fault planes shown in red, with striae in dashed stroke. Conjugate set and its stress directions, indicating a north to south to north-northeast to south-southwest shortening. In the stereo plot, the striae are shown in orange, and principal stresses derived from them in red, with a star for the main principal stress (σ_1). The steepness of the faults may indicate reactivation.* ***(C)*** *Outcrop 2. Neptunian clastic dyke of calcarenite shown in red intruded in limestone with regional bedding shown in yellow. The neptunian dyke has a present position of 272/83. Assuming horizontal bedding at the moment of deposition, the neptunian dyke developed vertically, and is an indicator of east-west extension.* ***(D)*** *Outcrop 3. Folded and faulted soft sediments in a syn-sedimentary ramp fold, verging north, indicating shortening in a 160-340 direction during the 144-150 Ma (latest Jurassic). Limestone showing regional bedding to the left and folded strata to the right (in yellow) and a reverse fault (in red). The soft sedimentary packet (with a sedimentary pattern) shows a chaotic character with no evidence of brechiation.* ***(E)*** *Outcrop 4. Map of the salt outcrop in the west and adjacent formations, showing the bedding strikes around the evaporitic body.* ***(F)*** *Outcrop 5. Reverse faults and folds with southeastern vergence, in a limestone outcrop situated less than 200 meters east of the outcropping salt. Regional bedding to the right and folded strata to the left are shown in yellow and reverse faults are shown in red. Rocks in the outcrop are not affected by halokinesis, and show signs of compressional deformation. The orientation of the fault planes and the axial planes of the folds are similar and indicate NNW-SSE shortening.*

Structures north of these outcrops seem to be exclusively related with the Alpine deformation phase. Approximately 200 m north of these outcrops, the Upper Jurassic shale and limestone layers (J5) dip north ("c" in Fig. 3A). Steep and sub-vertical N-dipping overturned layers alternate occasionally with S dipping beds ("d") for ~400 m in lower and middle Upper Jurassic rocks (J4). Bedding-parallel flexural slip associated with Alpine deformation is common and related striations show a N-S slip direction. Northward, Middle Jurassic (J3-J2) limestones and fine clastics dip consistently south until the topographic profile reaches its highest elevations ("e"). North of the topographic high, the orientation of Lower Jurassic strata (J1) changes from subvertical (~80˚) to subhorizontal with a gentle S-dip within a distance of ca. 500 m (Fig. 3A). Between the sub-vertical and sub-horizontal Lower Jurassic (J1) layers, S and N dipping sub-vertical strata alternate. Within this sector ("f" in Fig. 3A), highly deformed structures appear, showing faulted and folded strata, m-folds, recumbent folds, fault-related-folds, and more complex features, with unclear or non-sequential vergence. More to the north, the Lower Jurassic dolomites show no consistent strike for ~300 m, and layers are overturned (up to ~60˚) or S-dipping. Around 300 m east of the section, Upper Triassic evaporites (T) outcrop in a circular depression of approximately 1 km in diameter (Oc.4; Fig. 3E). An intrusive contact is seen between the evaporites and the lowermost Jurassic unit (J1). The Lower Jurassic bedding dips away from the outcropping evaporites, from sub-vertical nearby to 25˚ in a few hundred meters farther away from them. The strike directions of these Jurassic rocks vary consistently around the salt, in an overall concentric configuration. The strike directions progressively change to the

regional E−W to SW−NE trends 300-400 m away from the evaporites. Continuing north along cross-section A, overturned strata become subvertical (80˚-85˚) ("g") and finally N-dipping, before reaching the sub-horizontal Quaternary (Q) rocks that unconformably cover most of the northern flank. In this area, a sequence of SSE-verging fault-propagation folds outcrops in the Lower Jurassic limestones (J1), with axial planes indicating a SSE-to-NNW shortening direction (Oc5; Fig. 3F).

3.2 Central section: Cross-section B

Gently south dipping lower Middle Jurassic (J2) to lower Lower Cretaceous (C1) shales and limestones outcrop from the southern side of the anticline until significantly north of the topographic high (Fig. 4A). The oldest rocks seen in the section are Lower Jurassic (J1; shales) and outcrop ~1,5 km north of the topographic high, in the core of the anticline. North of the hinge of the anticline there are steep north dipping layers of lower Middle Jurassic (J2) to Lower Cretaceous (C1) age. Some of these steep layers are overturned and dip south ("i" in Fig. 4A). Further north, the Lower Cretaceous strata (C2-C3) have gentle north dipping slopes. The uppermost Upper Jurassic to lower Lower Cretaceous (J-C to C1) rocks are significantly thinner in the northern (~350 m) than in the southern (>900 m) flank along cross-section B (Fig. 4A).

In the southernmost of cross-section B, Quaternary (Q) deposits cover Lower Cretaceous rocks (C1-C3) ("a" in Fig. 4A). Northwards, rocks of the uppermost Upper Jurassic to lower Lower Cretaceous (J-C to C1) outcrop with consistent dips of ~40° to the south ("b"). Upper Jurassic (J4-J5) limestone layers have steeper dips that vary from ~40° to ~65° to the south ("c"). Further north, the Middle Jurassic (J2-J3) layers gradually decrease in steepness from ~45° to ~35° to the south ("d") and become roughly parallel to the topography ("e", dips of 10°-20° to the south) as they reach the topographic high.

Starting 300 m northwards of the topographic high, ~20° to 40° south dipping layers alternate with ~40° north dipping layers. This trend continues for ~400 m, and is seen also for parts of the Lower Jurassic (J1) rocks ("f"). Layers are folded asymmetrically in this area until the northward dips become dominant

(Oc.6; Fig. 4B). Advancing farther north, these Lower Jurassic (J1) shale-limestone layers overturn and dip south again, for a distance of more than 900 m. Dip angles of overturned Lower Middle Jurassic (J2) layers are here less verticalized than along the rest of this section (175°/73°) ("g"). The Jurassic rocks are locally underthrusted in a fault-bend fold structure that indicates top to the south motion (Oc.7; Fig. 4C). The layers remain sub-vertical for around 1100 m, and gradually decrease in steepness, from ~85° to ~50° to the north, in the lowermost Cretaceous (J-C) unit ("h"). Toward the north, layers of the lowest Lower Cretaceous (C1) are sub-vertical again, while the middle Lower Cretaceous (C2) strata have shallower dips (40° N) ("i") that decrease gradually to 20° N when reaching the upper Lower Cretaceous (C3) shales. Observations show no evidence of synsedimentary deformation in the limestones and marls of uppermost Upper Jurassic to lower Lower Cretaceous (J-C to C1) age along the cross-section B, but these units show a decrease of >500 m in thickness across the anticline strike (Fig. 4A).

Figure 4. Central section and main outcrops. ***(A)*** *Cross-section B.* ***(B)*** *Outcrop 6. Meter-scale fold in limestones at the location of main dip change in beds (shown in yellow) at the anticline axis.* ***(C)*** *Outcrop 7. Underthrust in overturned limestone strata. The fault is in red and beds are in yellow. Fault-bend fold, with top to the south movement, with 175/73 regional bedding. The fold in the hanging wall has a fold axis of 085/06 and axial plane of 022/14.*

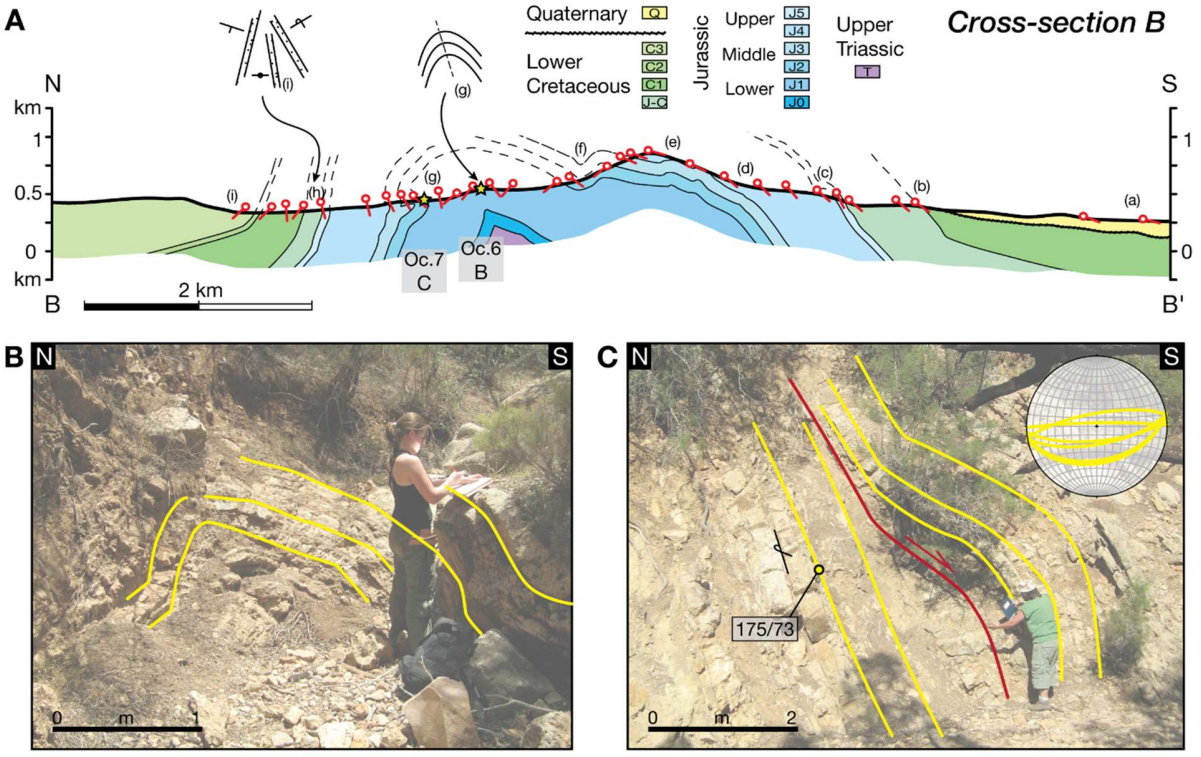

3.3 Eastern section: Cross-section C

Cross-section C portrays a north vergent anticline with two hinges, showing a northern steeply dipping flank and a southern gently dipping flank (Fig. 5A). The rocks exposed along this easternmost section are early Middle Jurassic (J2) to late Early Cretaceous (C3) in age. The thickness of the lowermost Cretaceous (J-C) formation varies from approximately 550 m on the southern flank to 400 m on the northern flank of the anticline, whereas the thicknesses of the Jurassic formations J2 to J5 are constant along the section.

In cross-section C, the southern flank of the Jbel Amsittene Anticline is characterized by south dipping sedimentary limestones, marls and shales ("a" in Fig. 5A), with subhorizontal Cretaceous rocks in its southernmost sector. Towards the north, older south-dipping carbonates crop out. Within the lowermost Lower Cretaceous – uppermost Lower Jurassic formation (J-C), layer inclinations vary between approximately 30° and 80° to the south ("b"). Here, the layers are locally offset by cm to dm-scale reverse

faults, which indicate N-S to NNE-SSW shortening coveal with sedimentation. Outcrop 8 (Fig. 5B) shows an example of these reverse faults in limestones. SSW dipping faults in this outcrop have up to ~20 cm offset and terminate in the slumped overlying sediments that show soft deformation, indicating a possible phase of syn-sedimentary deformation during the early post-rift of the Central Atlantic.

Outcrops farther north evidence deformation due to Alpine shortening. Towards the topographic high, the dip of the bedding gradually decreases from ~40° to 20° to the south, and upper Middle to middle Upper Jurassic (J3 – J4) rocks are exposed ("c"). Calcite-filled tension gashes are observed in several outcrops in and around the topographic high (Oc. 9; Fig. 5C). The veins are spaced by a few cm, and show both top-to-the-north and top-to-the-south shear kinematics. The former occurs mostly to the south of the topographic high, and the latter is observed mainly to the north of the topographic high. Northwards, along a ~500 m sector, the beds are subhorizontal gently dipping to the north ("d"). Approximately 1 km farther north, beds dip to the south for ~100 m before dipping north again ("e") and lower Middle Jurassic (J2) carbonates and sandstones are exposed. In the second topographic high, where the second hinge plane of the anticline intersects the topography, the orientation of the bedding is 65° to the north ("f"). Between the second topographic high and the valley north of the Jbel Amsittene Anticline, successive upper Middle Jurassic (J3) to lower Lower Cretaceous (C1) strata are exposed steeply dipping north (60-80°) ("g"). North of the valley, Lower Cretaceous (C1 to C3) limestone and marl strata are exposed dipping ~10 to 20° northwards ("h").

Figure 5. Eastern section and main outcrops. ***(A)*** *Cross-section C.* ***(B)*** *Outcrop 8. Inclined limestone layers cut by synsedimentary faults. High-angle reverse faults (in red) transect a thick bank (with its top and its bottom beds in yellow) with an offset of ~20 cm. The reverse fault tips end in the sedimentary layer on top that show soft sediment deformation of chaotic nature (in thin black), bracketing the age of deformation to 146-137 Ma (J-C formation, lowermost Lower Cretaceous – uppermost Lower Jurassic). The inclination of the reverse faults is suggestive of reactivation of former normal faults.* ***(C)*** *Outcrop 9. One of the two sets of sigmoidal tension gashes that outcrop at both sides of one of the anticline axes, in limestones. They indicate right lateral shear.*

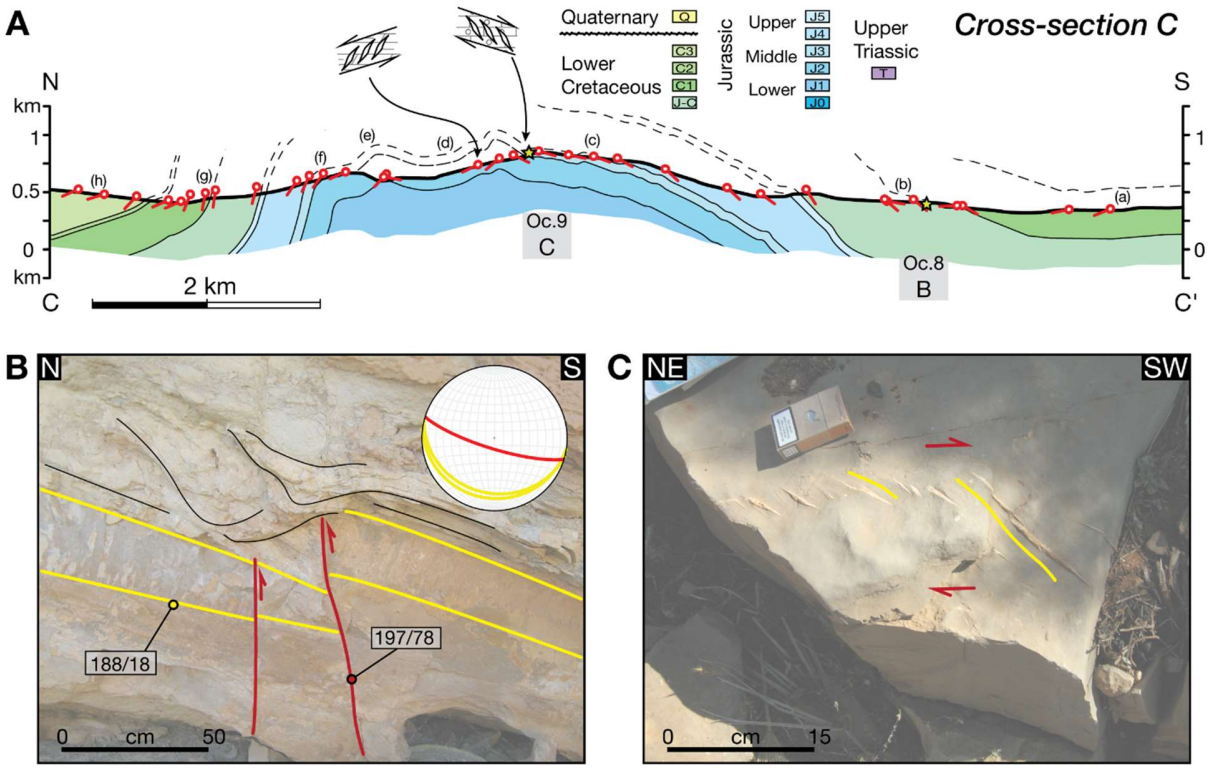

3.4 Eastern sectors of the Jbel Amsittene Anticline

Other relevant structural observations were found eastwards of the above-described sections. The most relevant structure for the scope of this study outcrops ~5 km to the east of cross-section C, in the lowermost Cretaceous (J-C) limestones (Oc. 10; Fig 6). This outcrop depicts a series of high angle reverse faults dipping SSW that transect limestones below a ~30 m long sedimentary wedge that pinches out towards the S. The top-to-the-north faults show reverse offsets of few to tens of centimeters and slickenlines indicating SSW-NNE shortening direction. The upper terminations of the faults are within the overlying lowermost Cretaceous syn-tectonic strata, and indicate active deformation during this period.

Figure 6. Outcrop 10. *Limestone outcrop showing an approximately 30 m long wedge pinching out towards the south, overlaying faulted strata. The top to the north-northeast faults have reverse offsets of a few to tens of centimetres that do not continue into the wedge, indicating a shortening direction of SSW-NNE during the J-C formation, lowermost Lower Cretaceous – uppermost Lower Jurassic. The steepness of the faults may be indicative of reactivation.*

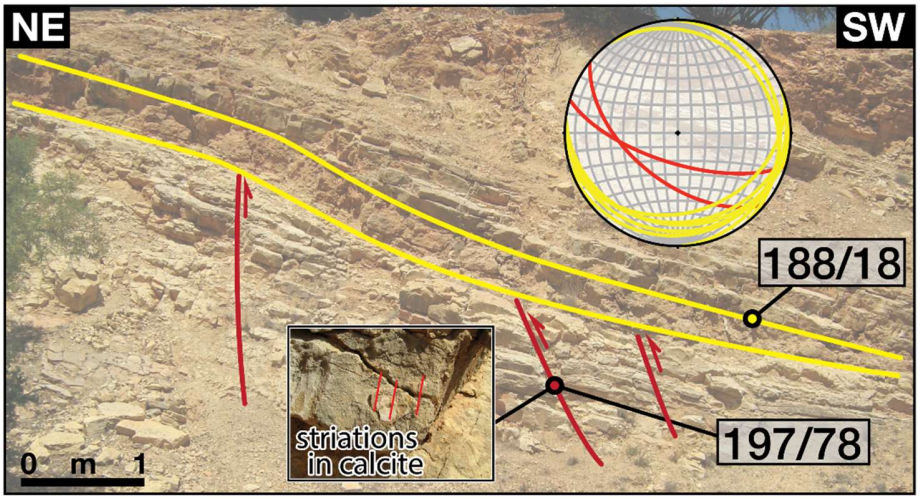

3.5 Structure and lateral variations in the Jbel Amsittene Anticline

We produced a structural map of the Jbel Amsittene (Fig. 7A). The map uses data collected from Section A to the coast, as in Brautigam et al, (2009), and two sections we reconstructed further east, where the anticline is more open (shown in Fig. 7B). These sections are similar in overall structure and geometry and change relevantly, albeit continuously, along the strike of the anticline (Fig. 7). The eastern sections (bottom of Fig. 7B) depict an open and asymmetrical anticline with a gentle north vergence. In the eastern sections (i) the southern limb dips gently and persistently south, (ii) salt deformation is not noticeable, neither in the hinge nor elsewhere, and (iii) the northern limb shows north dips with no overturned strata. The anticline shows a well-confined hinge and its flanks dip more gently than their western continuations. Small-scale structures are rare and more open. The layers along the limbs have an alternation of sectors with constant dip and sectors where dips vary progressively. By contrast, the western sections (top of Fig. 7B) present a tight structure and a clear north vergence. In the western sections, (i) the southern limb of the anticline dips south, from gently to steep, with local dips to the north, (ii) distortion by diapirism is limited to the vicinity of the hinge where the salt is outcropping, and (iii) the northern limb is frequently overturned and partly covered by Quaternary deposits. The western sections show a topographic crest characterized by a north tête-plongeante geometry. Strain markers are numerous and strata often show relevant changes in dip direction over short horizontal distances.

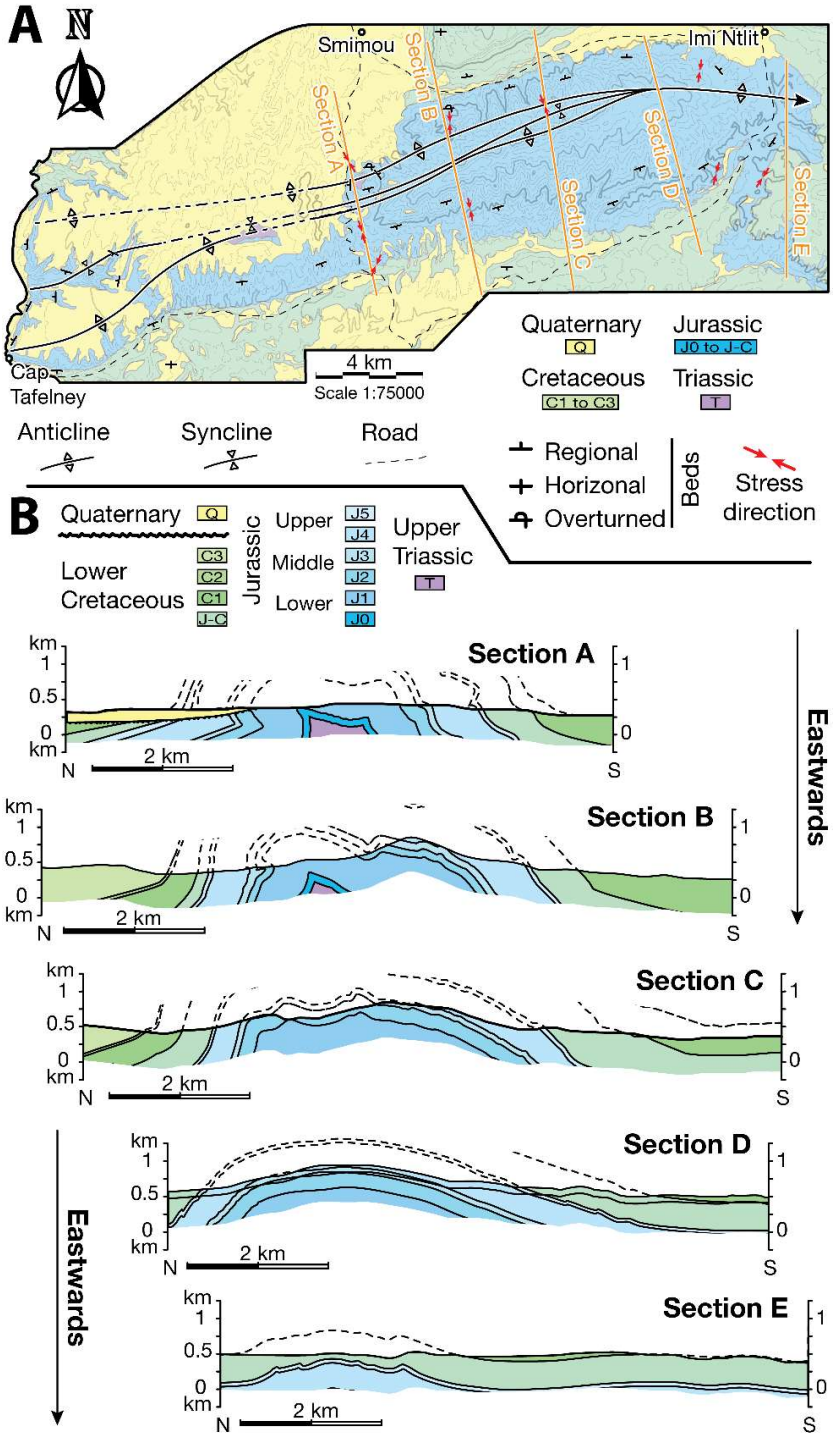

Figure 7. Structure of the Jbel Amsittene Anticline. ***(A)*** *Structural map showing the main axis of the anticline, which bifurcate westwards, and its plunge towards the east. The map also shows the regional bedding dips in the different sectors of the anticline. The full bedding dip data collected in the fieldwork are provided in the Supplementary Material. Contours in grey represent lines of equal height every 50 m, with darker tones and thicker strokes for the heights of 250 m, 500 m and 750 m.* ***(B)*** *Geological sections in the Jbel Amsittene Anticline, from west to east, showing the anticline structure and vergence and its lateral variations.*

3.6 Thickness changes along the Jbel Amsittene

To obtain thickness variations in the Jurassic formation, we put forward a 3D thickness model integrating remote sensing (horizon mapping) and structural data (dip data and geological cross sections; Fig. 8). We used a "3 point-solver" plug-in for Google EarthTM to derive bed attitude from the contact between beds and topography at three or more points (Bennison and Moseley 2003). With these means, we collect dip data of bed contacts tens of meters in scale, at various locations around the anticline. We mapped horizons on DEM-coupled satellite images (Google Earth Pro^{TM}) to obtain spatial coordinates of well-exposed geological contacts, identified by the georeferenced geological map of Choubert (1965) and color changes in the imagery. We used the mapped horizons and the large-scale (tens of meters) dip data in geological cross-sections to derive a 3D model of continuous stratigraphic surfaces using *StructuralLab* tool of *Gocad*. We then used the *kine3d-1* tool and *Matlab* to obtain true thickness maps from the mapped horizons. Model resolution suggests a precision of ~20 m at the surface, and hence lies below the thinnest stratigraphic units within the study area.

Thickness maps reveal an along-strike change in the thickness of Jurassic rocks (Fig. 8). Thickness variations comprise the Lower Jurassic (J0, J1), Middle Jurassic (J2, J3), and Upper Jurassic (J4, J5) along a clockwise profile from the northwestern to the southwestern fold flanks. We find maximum unit thicknesses in the overturned northern flank and a decrease in thicknesses eastwards. Such thickness decrease is substantial at the point where the fold limbs change into NNW dipping beds. All formations follow this trend, that becomes less significant towards the Upper Jurassic (J4, J5). It is worth noticing, however, that modeling is less precise in overturned layers. In the southern limbs, towards the west, thicknesses in all formations increase progressively, albeit remaining below thicknesses of the northern limb (Fig. 8). Generally, thicknesses are never constant along the anticline strike for >5 km. Thickness at the eastern side are around 40 to 50 m in J3 and 140 m and 80 m in J4, respectively. Sediments increase in thickness towards the southern limbs, with 140 m to 200 m for J3. This corresponds to a thickness increase of ~70-75%. The J4a (Oxfordian) strongly increases from around 140 m to more than 300 m.

Figure 8. Thickness model. (A/B/C) *Model of thickness variations along contour likes of three Upper Jurassic sequences. (D) Modelled thickness variations of Jurassic rocks in a clockwise profile from the northwestern to the southwestern flank of the anticline.*

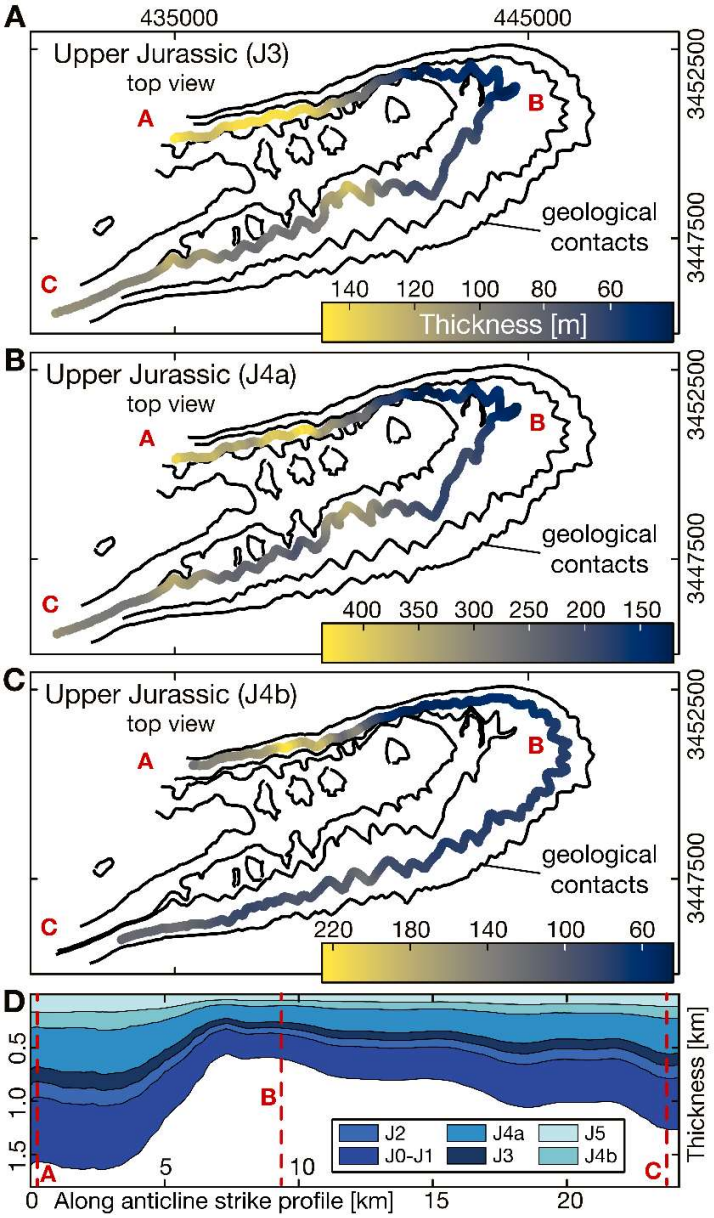

We also derive thicknesses for the upper Upper Jurassic - Lower Cretaceous units (J-C, C1, and C2) using bed attitudes along unit contacts. We use this input to infer the planes of contact between the sedimentary units and calculate true thicknesses by measuring the distance between contacts orthogonally. Although this approach is less accurate and lacks the along-strike coverage of the aforementioned thickness

model, it provides a valid first-order estimate on the variation of sedimentary thickness across strike. The upper Upper Jurassic - Lower Cretaceous units (J-C, C1, and C2) decrease in thickness northwards across the strike of the Jbel Amsittene Anticline (Table 1). As seen in cross-sections A and B (Figs. 4 & 5), formations J-C and C1 are up to ~350 m thinner in the northern flank with respect to the southern flank of the anticline (Table 1). These values represent a minimum estimate, given that the upper boundary of C1 is in places outside the limits of our study area. Our observations suggest that sedimentary thickness changes affect C2 as well, and that no thickness changes affect the Lower Cretaceous C3 formation. These thickness variations are less obvious in the east of the study area (Fig. 7).

	Formation J-C		Formation C1	
	N flank	S flank	N flank	S flank
Cross-section B	150m	500m	350m	500m
Cross-section C	400m	650m	350m	450m

Table 1. *Thickness changes between the northern and the southern flank of the Jbel Amsittene Anticline for formations J-C and C1.*

4 Discussion

4.1 Key characteristics of the Jbel Amsittene Anticline

The Jbel Amsittene Anticline has a limited lateral extent and shows geometry changes along strike (Fig. 7). In the west, the anticline manifests as a box anticline with a gentle north vergence within a broader area of deformation. The anticline continues westwards into the offshore for less than ~10 km off the coastline (Hafid, 2006). The tight tête-plongeante that the anticline has in the west smoothens and widens into an open fold (up to ~20 km in wavelength) and wanes eastward, as the axis of the anticline plunges eastwards (Fig. 7). As a result of an eastward plunge of the fold axis and the southward dip of its axial plane, the oldest rocks at the core of the anticline are exposed in the west and located to the north of the topographic high.

Thickness variations have different trends in Jurassic and Early Cretaceous units. Jurassic units show a signal of eastward decreasing thicknesses along strike and with maxima in the anticline center (Fig. 8). The cumulative thickness for the Jurassic units has sharp variations of up to 900 m between the northern flank and the eastern termination of the anticline, while between the latter and the southern flank, thickness variations are of ~600 m. A second-order signal across the anticline strike portrays a decrease in thickness towards the southern flank (Fig. 8). The combined thickness of units J-C and C1 decreases by up to 500 m northwards, across the axis of the anticline, and by up to 250 m eastwards over a short distance (Table 1). Whereas thickness changes in Jurassic units seem unrelated to a tectonic event, the latter units may relate to changes in shortening rates, as shown below.

Differential strain distribution along the anticline strike can be inferred for modern and antecedent forms of the Jbel Amsittene Anticline. We derive along-strike changes in amount of shortening from variations in line-length approximations along the present anticline strike and from the number and size of outcrop-scale syn-sedimentary structures in the Upper Jurassic – lower Lower Cretaceous (J-C) formation (Table 2). The western section presents line-length shortening values of ~1,6 km over a measured length of ~7,6 km, i.e., ~21% shortening. This shortening value remains almost constant in the central section (~20 %), and decreases in the eastern section (14,5 %). Farther east, in the easternmost section, we measured 0,2 km of shortening over a length of ~4,3 km, i.e. ~4,5 % shortening (Table 2). Thus, line-length shortening decays along the Jbel Amsittene Anticline strike from its center to the east. Although most deformation and probably the observed eastward decay in shortening along the anticline strike relates to structure tightening during Alpine times, we infer a similar trend for the syn-depositional structures in the Upper Jurassic – lower Lower Cretaceous (J-C) formation. Most of such syn-depositional structures appear in the west of the anticline and are absent in coveal rocks in the east and of upper Lower Cretaceous (C3) age exposed in the northern part of the study area. This suggests that the eastwards decrease in shortening resulted in a westward-opening conical anticline, by the end of the Lower Cretaceous (C3).

	Deformed length (km)	Shortening (km)
Cross-section A	7,6	1,6
Cross-section B	9,5	2,1
Cross-section C	10,3	1,5
Cross-section D	9,1	0,6
Cross-section E	4,3	0,2

Table 2. *Decrease in amount of shortening to the east, measured as unfolded line-length.*

Syn-sedimentary deformation is common in outcrops of the uppermost Upper Jurassic-lowermost Cretaceous limestones (J-C), and is expressed as clastic dykes, fault-related folds and reverse faults affecting soft sediment (Figs. 3, 4, 5 & 7). Overall top-to-the-north steep reverse faults with tips that offset soft sediments by few to tens of centimeters (Figs. 5 & 6) suggest N-S to NNE-SSW shortening. This observation can be coupled with striae in nearby conjugate fault sets indicating NNW-SSE to NNE-SSW maximum horizontal stresses (Fig. 6). Other equivalent coeval reverse faults are also steep in their pre-rotated stages, and probably result from reactivation of Triassic–Liassic normal faults. Similar evidence of syn-sedimentary shortening during deposition of the J-C unit can be found along the anticline strike. However, regional layer dips for this unit vary greatly (between approximately 30° and 80°), and evidence in other outcrops, such as the tête-plongeante or the overturned strata, are clear indications of younger shortening. Taken together, the data suggest that shortening during the early post-rift phase of the Central Atlantic initiated anticline growth of the Jbel Amsittene, and that the anticline further developed and tightened during the Alpine orogeny (e.g., Saura et al., 2013 in the Central High Atlas; Pichel et al., 2019b in the offshore Essaouira-Agadir Basin; this study, in the Jbel Amsittene).

4.2 Models for the evolution the Jbel Amsittene Anticline

We put forward two potential models for the evolution of the Jbel Amsittene Anticline in Mesozoic times. We discuss, on the basis of the evidence presented in this contribution, our preferred model for an initial Mesozoic anticline development, which was enhanced and partly overprinted in the Cenozoic. Comparative, detailed structural studies inclusive of similar onshore anticlines in the area are required to

confidently discriminate among these two potential evolutionary models proposed for the Jbel Amsittene Anticline, and elucidate the underlying growth mechanism for equivalent structures in the Moroccan margin. Discrimination among different the models would have implications on the geodynamic causes controlling the anomalous vertical motions during the early post-rift phase along the African margin.

In the first scenario, we assume the diapiric rise of the Triassic salt at the core of the present anticline is the driving force leading anticline growth already during the Early to Middle Jurassic. Halokinesis and salt tectonics are well expressed in the area (Hafid et al., 2006; Hafid, 2000) and proposed to happen during this period in the Central High-Atlas (Saura et al., 2013) and in the offshore Essaouira-Agadir Basin (Pichel et al., 2019a). Although extensive diapirism exists offshore Morocco, no clear interpretations of pre-Cretaceous timing and mechanism(s) of salt mobilisation are available, and it thus may occur in relation to different mechanisms than in the onshore (Neumaier et al., 2016). Moreover, salt mobilisation may potentially lead to syn-sedimentary deformation along the sides of the diapir and sedimentary dykes (Morley et al., 1998; Giles and Lawton, 2002 respectively; see examples in Poprawski et al., 2014). The Late Jurassic-Early Cretaceous deformation features may therefore be gravity-driven sedimentation features of local origin that can form on any submarine slope of a few degrees.

Many syn-sedimentary faults observed in the field are very steep. Although this might be the result of fault measurements concentrating on the steep, upper tips of the faults, none of the faults has its root exposed. Moreover, the upper tips seem to show a sharp termination, potentially lithology-controlled. Is it possible that these faults are intraformational, and that they, and folded units, were generated by shear stresses of individual sedimentary packages sliding along bedding planes. This could be associated with slope gravity processes or a rising salt diapir, but this is unlikely given that some of these structures have vergence towards the diapir. Slope oversteepening can be purely sedimentary, and tectonic processes do not have to be involved to explain their formation. In this scenario, vertical movements (Stets, 1992; Bertotti and Gouiza, 2012; Gouiza et al., 2017) could be linked to anticline fold growth and salt tectonics, such that a gravitational load is applied by the uplift of the High Atlas and by the subsiding continental margin,

creating a hydraulic head and consequent salt activation (Pichel et al., 2019a). The presence of salt in the anticline core and Jurassic thickness variations along the anticline that do not relate to the present structure are potential indicators for such salt-driven scenario, although further evidence from nearby anticlines need to be found.

In the second scenario, we assume that the Jbel Amsittene Anticline initially formed by horizontal shortening in the latest Jurassic and earliest Cretaceous. Horizontal shortening would mark an initial period of contraction and folding during the early post-rift phase, leading to the syn-tectonic growth of sedimentary wedges at anticline and outcrop scales (Figs. 4 & 5). Shortening would have started during latest Jurassic – earliest Cretaceous (J-C) and continued during the deposition of the Lower Cretaceous unit (C1), and finally ended before unit C3 deposition. During this time, the Jbel Amsittene developed as an open anticline that was probably asymmetrical along strike. The Triassic salt would function as a weak detachment facilitating accommodation of the horizontal stresses that lead to the reactivation of pre-existing structures (e.g., basement rift-related faults) and initial anticline growth before Cretaceous-Cenozoic tectonics (Hafid et al., 2006; Tari et al., 2003; Hafid, 2006). This shortening tectonics would be consistent with field observations of syn-sedimentary structures in the J-C unit as well as the existence of structures with clear vergence tens of meters away from the outcropping salt with limited strain (Fig. 3) near its contact. The lack of coherency in trend or scale of the salt with the overall anticline structure are also indicators of absence of halokinesis in the Jbel Amsittene during early post-rift of the Central Atlantic. These observations imply that Triassic salts were mobilised during compression led by horizontal tectonic forces, and that the growth of associated structures occurred in relation to a blind thrust rooted in the Triassic salt. The tête-plongeante structure towards the west and overturned layers at some sites indicate further shortening and anticline tightening during Alpine times. These structures and their consistent change along strike (Fig. 7) argue for vertical anticline growth during two overprinting phases of shortening, both acting roughly in the N-S direction. We thus consider that the evidence reported here favors the second scenario by which the latest Jurassic – earliest Cretaceous growth of the Jbel Amsittene occurred by tectonic shortening.

The ENE-WSW strike of the Jbel Amsittene Anticline is parallel to the strike of the major structures bounding the High Atlas belt (Fig. 1B). These structures activated under a transtensional regime during the Triassic-Early Jurassic rifting, and defined several pull-apart basins where grabens and half-grabens, bounded by N- to NE-trending normal faults related to rifting of the Central Atlantic, were filled by terrigenous and evaporitic series (Piqué et al., 2002; Laville et al., 2004; Frizon de Lamotte, 2005). In our attempt to reconstruct the evolution of the Jbel Amsittene through time, we hypothesize that the Jbel Amsittene Anticline formed in strata overlying a previous half-graben structure bounded by an E-dipping normal fault to the east and an E-W left-lateral strike slip fault to the north (Figs. 1B & 9). The latter is shown in the Mesozoic structural map of the Essaouira-Agadir Basin by LeRoy & Pique (2001), based on seismic data. The presence and relative accommodation space expected from both these pre-existing structures could explain increasing Jurassic thicknesses westwards and northwards along and across anticline strike, respectively (Figs. 7 & 8). We interpret the upwards decreasing thickness in Upper Jurassic units (Fig. 9) as an indication that the aforementioned faults were sealed, at the latest, by the end of the Late Jurassic (rifting kinematics, for both High Atlas and Central Atlantic, end in the Early Jurassic; e.g., Michard et al., 2008). Subsequent Late Jurassic-Early Cretaceous folding of the Jbel Amsittene Anticline may have occurred by reactivation of the E-W structure as a blind thrust, as interpreted on the structural map of Hafid et al., (2006) and on their seismic interpretation. This would result in thicknesses that increase towards the hanging-wall, i.e. southwards across the anticline, and are thus opposite in trend with regards to those in the Jurassic units (Table 1). Such blind thrust would be rooted in Triassic evaporites, acting as a weak decollement layer between the basement and the overlying Mesozoic basin infill (Fig. 9). Therefore, most of the strain was localised in the depocentre of the Triassic salt found underneath the western part of the Jbel Amsittene and wedging out towards the east. This is coherent with eastwards decreasing strain observed for both the early post-rift and the Alpine shortening phases.

Figure 9. Evolutionary model of the Jbel Amsittene Anticline. *Proposed evolutionary model of the Jbel Amsittene Anticline. In the last time-step we show the anticline with its finite geometry at present, which also results from Alpine tectonism.*

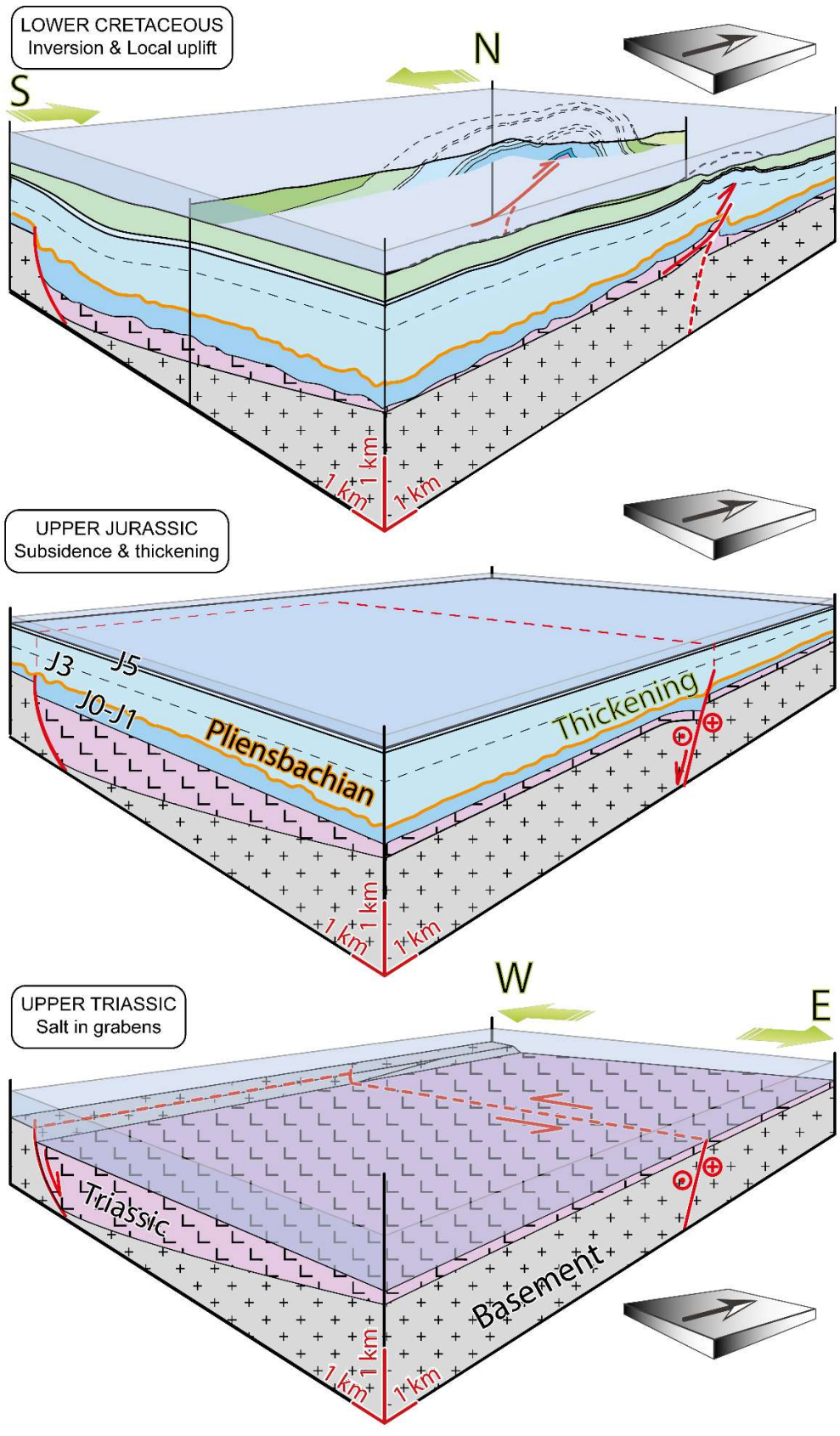
LOWER CRETACEOUS
Inversion & Local uplift
N
S
1 km
1 km
1 km
UPPER JURASSIC
Subsidence & thickening
J3
J5
J0-J1
Pliensbachian
Thickening
1 km
1 km
1 km
UPPER TRIASSIC
Salt in grabens
W
E
Triassic
Basement
1 km
1 km
1 km

4.3 Regional shortening in other Moroccan sites during anticline growth

Observations within and nearby the Essaouira-Agadir Basin, suggest that some of the other salt structures present in the rifted margin may have been originally formed at earlier times than the Tertiary contraction (Hafid et al., 2006; e.g., Bertotti and Gouiza, 2012; Saura et al., 2013; Benvenuti et al., 2017; Moragas et al., 2018; Pichel et al., 2019a). This could be the case of the Tidsi Anticline and the Imi n'Tanout wedge in the Essaouira-Agadir Basin (Fig. 1B), and the Dadès Valley in the Ouarzazate Basin. These structures may have formed similarly to the Jbel Amsittene Anticline, i.e. during an early post-rift shortening phase that reactivated inherited structures in assistance of the Triassic evaporitic rocks (Fig. 9). However, truncation of the basalt horizons by the Pliensbachian unconformity within certain structures also suggest the presence of earlier salt growth (Hafid et al., 2006).

The Tidsi Anticline, north of the Jbel Amsittene Anticline (Fig. 1B), was also thought to result from salt diapirism during the Late Cretaceous. The main arguments are the presence of growth strata documented in the Upper Cretaceous rocks and the lack of Jurassic series, coupled with the absence of tectonic indicators associated with these growth features (Amrhar, 1995; Hafid, 2006). While the relevance of diapirism in controlling the growth of the Tidsi Anticline during Late Cretaceous time is not unlikely, other older structures are observed in the area which document the existence of Early Cretaceous tectonic deformations hitherto neglected (Bertotti and Gouiza, 2012). This study also documents that the Late Lower Cretaceous strata in the uppermost part of the outcrop are sub-horizontal, which implies deformation occurred prior to the Late Cretaceous. The tectonic nature of these structures is proven by the fold vergence towards the core of the Tidsi Anticline, which is incompatible with an halokinetic origin.

To the east of Jbel Amsittene, the geometry of the post-rift portion of the Imi n'Tanout wedge (Fig. 1B) prior to Alpine shortening has been reconstructed coupling thickness measurements with structural field observations (Zühlke et al., 2004; Bertotti and Gouiza, 2012). These studies show syn-depositional deformation is common in the Imi n'Tanout wedge at the outcrop scale, and folds and thrusts with a NW-

SE trending axis are common. These structures document Late Jurassic to Early Cretaceous NE-SW shortening approximately perpendicular to the axis of the Imi n'Tanout wedge suggesting their formation within the same deformation regime. Shortening structures are conformal to the large-scale folds in the northern part of the Essaouira-Agadir Basin that are related to the inversion of the Atlas system.

In the Ouarzazate foreland basin, located ca. 300 km southeast of the Essaouira-Agadir Basin and south of the central High Atlas (Fig. 1A), there is also strong evidence for a pre-Atlasic shortening event (Benvenuti et al., 2017). Observations from the Dadès Valley indicate angular and progressive unconformities of syn-tectonic character within the Middle Jurassic to Lower Cretaceous stratigraphic units (Benvenuti et al., 2017). This study also documents syn-sedimentary tectonic structures that suggests a first Middle Jurassic-Early Cretaceous NNE-SSW to NNW-SSE shortening and a later E-W shortening during the Late Cretaceous (Benvenuti et al., 2017).

4.4 Vertical motion and horizontal deformation during anticline growth

A review of the temporal and spatial distribution of the crustal vertical movements has led to the proposal of an overall exhumation/subsidence history for Morocco and its surroundings (Charton et al., 2018). Present-day basement massifs surrounding the Essaouira-Agadir Basin, i.e. the Anti-Atlas, the Marrakech High Atlas, and the Meseta, have been active sources of sediments sporadically throughout the Mesozoic (Fig. 10). Specifically, the Anti-Atlas, south of the Jbel Amsittene area underwent significant exhumation between the Triassic and Middle Jurassic and during the Late Cretaceous to Present-day, while the Meseta and High Atlas massifs were exhumed from the Middle Jurassic to the Early Cretaceous and towards the end of the Late Cretaceous. This discrepancy in exhumation time led to substantial shifts in source areas, yet to be tested with sedimentary provenance analysis in the Essaouira-Agadir Basin.

Contractional structures in the Cretaceous sedimentary units of the Essaouira-Agadir Basin are coeval with major rearrangements in plate motions related to the opening of the South and North Atlantic

Ocean (Fig 10). Continental separation and accretion of oceanic crust in the South Atlantic (Torsvik et al., 2009), between SW Africa and South America, as well as in the southern segment of the North Atlantic (Knott et al., 1993; Tucholke et al., 2007), between Iberia and Newfoundland, started in the Aptian-Albian time. We propose that the resulting counterclockwise rotation of Africa and the southward drifting of Iberia led to N-S compressive stresses within the African plate. At the same time, the ongoing oceanic accretion and mid-Atlantic ridge push in the Central Atlantic resulted in E-W compressive stresses (e.g., Gouiza et al., 2019). Similarly, another Mesozoic failed rift system between northwest and southern Africa along the Atlantic margin was active in the Early Cretaceous (e.g., Guiraud and Maurin, 1992) that may have triggered N-S far-field stresses in Morocco.

The steady acceleration of the Atlantic Mid-Oceanic ridge spreading during the Jurassic period is a known active process in the Central-Atlantic region that may lead to tectonic stresses (Fig. 10C; Labails et al., 2010). Several drivers of the erosional exhumation were at work in the Jurassic: (a) relatively low sea level (e.g., Snedden and Liu, 2010); (b) far-field intraplate stresses by Mid Oceanic Ridge push; (c) positive dynamic topography (up to 100 m of surface uplift; Barnett-Moore et al. 2017) potentially leading to regional instabilities; (d) high paleo-latitudes (similar to those of the Present-day; after Scotese 2016; Fig. 10C) and; (e) arid to humid climates in the High Atlas during the Early Jurassic (Wilmsen and Neuweiler, 2007). Some of these processes, or some combination of them, may be responsible for the documented exhumation, and could have resulted in the instability and mobilisation of the Triassic salt by erosion of the sedimentary cap, generating hydraulic heads from East to West with surface uplifts in the surrounding massifs, or the propagation of faults in the salt cap generated by far-field intraplate stresses and/or surface uplift.

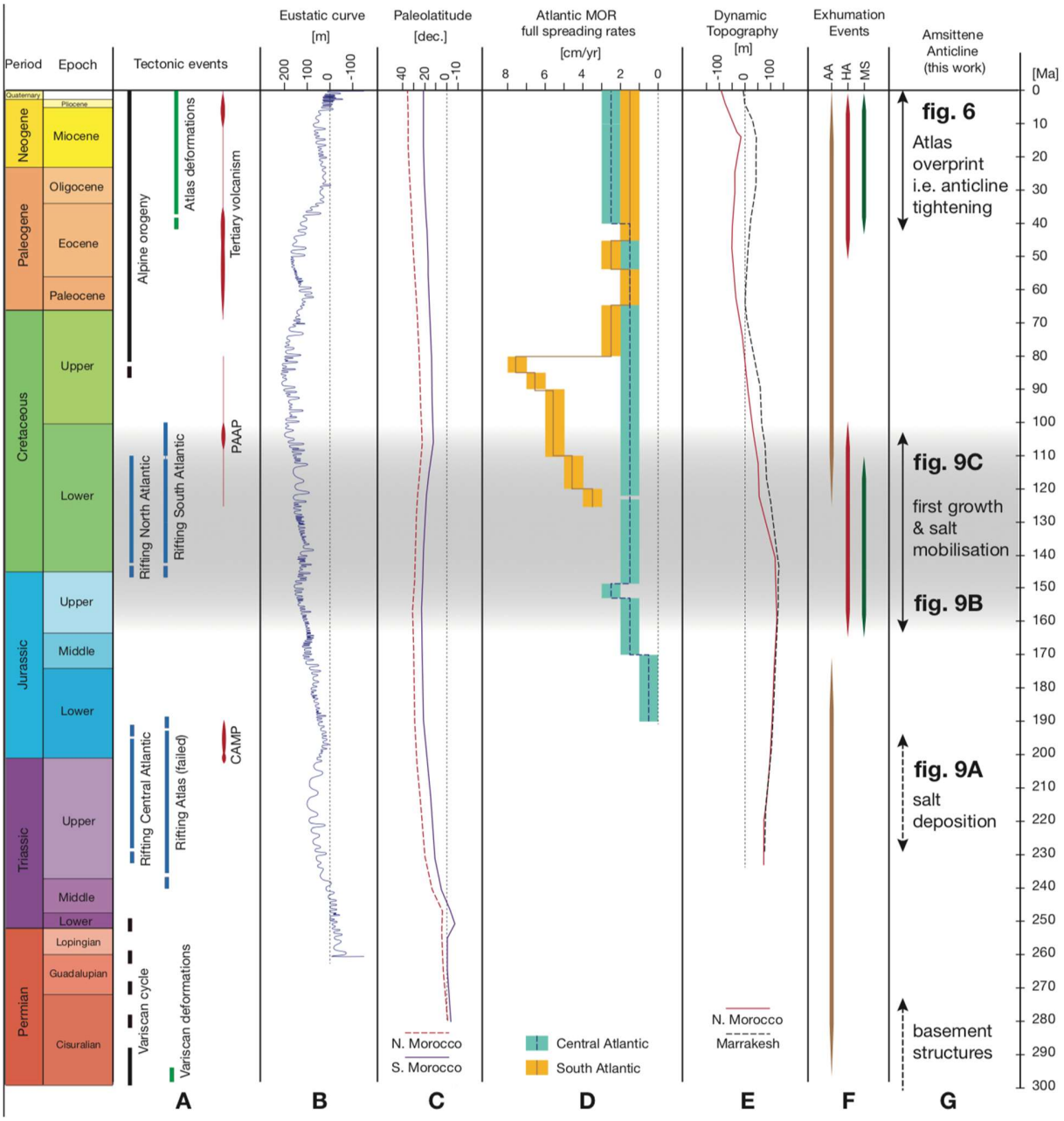

Figure 10. Time chart and compilation for the Jbel Amsittene Anticline. ***(A)*** *Tectonic events (after Charton, 2018 and the references therein);* ***(B)*** *Sea level (after Snedden and Liu, 2010);* ***(C)*** *Paleolatitude (after maps of Scotese, 2016);* ***(D)*** *Full mid oceanic ridge spreading rates (compiled in Charton, 2018);* ***(E)*** *Dynamic topography for two points in Morocco (from GPlates website, after modle CIs of Barnett-Moore et al. (2017);* ***(F)*** *Exhumation events as compiled in Charton (2018; see references therein);* ***(G)*** *Evolution of the Jbel Amsittene (this work). CAMP; Central Atlantic Magmatic Province; PAAP: Peri-Atlantic Alkaline Pulse.*

The spatial and temporal relation between these contractional structures and the regional uplift event that affected the NW African margin suggest a common genetic process (Ghorbal et al., 2008; Leprêtre et al., 2015b; Gouiza et al., 2017; Charton et al., 2018). We consider that Late Jurassic-Early Cretaceous shortening in the Essaouira-Agadir Basin was driven by these N-S and E-W compressive stresses that reactivated the E-W (High Atlas/Tethysian failed rift) and N-S (Central Atlantic rift) syn-rift structures alike, and later initiated subsequent salt movements onshore and offshore the Moroccan rifted margin (Hafid et al., 2006; Hafid, 2000, 2006; Tari et al., 2003).

5. Conclusions

We collected detailed structural evidence in the Jbel Amsittene. Our data indicate that the structure is an asymmetrical and north-verging anticline, with a northern flank that dips steeply and locally overturns, and a southern flank that dips south more gently. Our data suggest that the Jbel Amsittene Anticline is a fault-propagation-fold with its detachment plane rooted in Late Triassic evaporites, that initially grew during NNW-SSE shortening by the end of the Late Jurassic. Shortening led to anticline-scale and outcrop-scale syn-tectonic wedges in Late Jurassic and Early Cretaceous strata and outcrop-scale syn-sedimentary structures indicating compressional stresses. The anticline lacks structures related to diapiric rise at relevant scales and the effect of salt diapirism is restricted locally to an area around the anticline core. We therefore conclude that the initial development of Jbel Amsittene Ancline during Late Jurassic-Early Cretaceous times was mainly driven by shortening led by compressional tectonics, and only partially the result of salt tectonics, despite the promotion of halokinetic drivers described in recent literature. Later inversion of the Atlas system since the Late Cretaceous caused the tightening of the anticline. Being one of many contemporaneous contractional structures reported in the Essaouira-Agadir Basin and nearby basins linked to crustal-scale Middle Jurassic to Early Cretaceous exhumation, our observations suggest a tectonic evolution driven by intraplate stresses along the entire NW African margin.

Acknowledgements

Authors would like to thank the careful reviews by two anonymous colleagues on a previous version of the manuscript. DFB wants to thank the Vrije Universiteit Amsterdam for funds that partially covered fieldwork expenses of this work, part of his M.Sc. Thesis.

Figures

Figure 1. Maps of tectonic provinces and geology. (A) Regional map of Morocco showing the major tectono-stratigraphic provinces and basins of coastal Western Morocco (simplified from the geological map of Morocco; Hollard et al. 1985). With indication of the location of Panel B. **(B)** Geological map of the western High Atlas and Essaouira-Agadir Basin showing the main Triassic-Liassic rift-related structures near the Amsittene Anticline (Hollard et al. 1985; Le Roy and Piqué 2001).

Figure 2. Geology and chronostratigraphy in the Jbel Amsittene Anticline. (A) Geological map of the Jbel Amsittene Anticline, showing the location of the main observations in the field (yellow stars) and cross-sections that have been used to constrain the geological evolution of the area. Outcrops and outcrop numbers are shown as Oc.#. **(B)** Simplified chronostratigraphic and environmental column of the Jbel Amsittene area. Based on Hafid (2000), the geological map of Tamanar from the Moroccan Geological Survey and Zühlke et al. (2004).

Figure 3. Western section and main outcrops. (A) Cross-section A. **(B)** Outcrop 1. Limestones with regional bedding shown in yellow and faults and fault planes shown in red, with striae in dashed stroke. Conjugate set and its stress directions, indicating a north to south to north-northeast to south-southwest shortening. In the stereo plot, the striae are shown in orange, and principal stresses derived from them in red, with a star for the main principal stress (σ_1). The steepness of the faults may indicate reactivation. **(C)** Outcrop 2. Neptunian clastic dyke of calcarenite shown in red intruded in limestone with regional bedding shown in yellow. The neptunian dyke has a present position of 272/83. Assuming horizontal bedding at the moment of deposition, the neptunian dyke developed vertically, and is an indicator of east-west extension. **(D)** Outcrop 3. Folded and faulted soft sediments in a syn-sedimentary ramp fold, verging north, indicating shortening in a 160-340 direction during the 144-150 Ma (latest Jurassic). Limestone showing regional

bedding to the left and folded strata to the right (in yellow) and a reverse fault (in red). The soft sedimentary packet (with a sedimentary pattern) shows a chaotic character with no evidence of brechiation. **(E)** Outcrop 4. Map of the salt outcrop in the west and adjacent formations, showing the bedding strikes around the evaporitic body. **(F)** Outcrop 5. Reverse faults and folds with southeastern vergence, in a limestone outcrop situated less than 200 meters east of the outcropping salt. Regional bedding to the right and folded strata to the left are shown in yellow and reverse faults are shown in red. Rocks in the outcrop are not affected by halokinesis, and show signs of compressional deformation. The orientation of the fault planes and the axial planes of the folds are similar and indicate NNW-SSE shortening.

Figure 4. Central section and main outcrops. (A) Cross-section B. **(B)** Outcrop 6. Meter-scale fold in limestones at the location of main dip change in beds (shown in yellow) at the anticline axis. **(C)** Outcrop 7. Underthrust in overturned limestone strata. The fault is in red and beds are in yellow. Fault-bend fold, with top to the south movement, with 175/73 regional bedding. The fold in the hanging wall has a fold axis of 085/06 and axial plane of 022/14.

Figure 5. Eastern section and main outcrops. (A) Cross-section C. **(B)** Outcrop 8. Inclined limestone layers cut by synsedimentary faults. High-angle reverse faults (in red) transect a thick bank (with its top and its bottom beds in yellow) with an offset of ~20 cm. The reverse fault tips end in the sedimentary layer on top that show soft sediment deformation of chaotic nature (in thin black), bracketing the age of deformation to 146-137 Ma (J-C formation, lowermost Lower Cretaceous – uppermost Lower Jurassic). The inclination of the reverse faults is suggestive of reactivation of former normal faults. **(C)** Outcrop 9. One of the two sets of sigmoidal tension gashes that outcrop at both sides of one of the anticline axes, in limestones. They indicate right lateral shear.

Figure 6. Outcrop 10. Limestone outcrop showing an approximately 30 m long wedge pinching out towards the south, overlaying faulted strata. The top to the north-northeast faults have reverse offsets of a few to tens of centimetres that do not continue into the wedge, indicating a shortening direction of SSW-NNE during the J-C formation, lowermost Lower Cretaceous – uppermost Lower Jurassic. The steepness of the faults may be indicative of reactivation.

Figure 7. Structure of the Jbel Amsittene Anticline. (A) Structural map showing the main axis of the anticline, which bifurcate westwards, and its plunge towards the east. The map also shows the regional bedding dips in the different sectors of the anticline. The full bedding dip data collected in the fieldwork are provided in the Supplementary Material. Contours in grey represent lines of equal height every 50 m, with darker tones and thicker strokes for the heights of 250 m, 500 m and 750 m. **(B)** Geological sections in the Jbel Amsittene Anticline, from west to east, showing the anticline structure and vergence and its lateral variations.

Figure 8. Thickness model. (A/B/C) Model of thickness variations along contour likes of three Upper Jurassic sequences. **(D)** Modelled thickness variations of Jurassic rocks in a clockwise profile from the northwestern to the southwestern flank of the anticline.

Figure 9. Evolutionary model of the Jbel Amsittene Anticline. Proposed evolutionary model of the Jbel Amsittene Anticline. In the last time-step we show the anticline with its finite geometry at present, which also results from Alpine tectonism.

Figure 10. Time chart and compilation for the Jbel Amsittene Anticline. (A) Tectonic events (after Charton, 2018 and the references therein); **(B)** Sea level (after Snedden and Liu, 2010)**; (C)** Paleolatitude

(after maps of Scotese, 2016); **(D)** Full mid oceanic ridge spreading rates (compiled in Charton, 2018); **(E)** Dynamic topography for two points in Morocco (from GPlates website, after modle CIs of Barnett-Moore et al. (2017); **(F)** Exhumation events as compiled in Charton (2018; see references therein); **(G)** Evolution of the Jbel Amsittene (this work). CAMP; Central Atlantic Magmatic Province; PAAP: Peri-Atlantic Alkaline Pulse.

Tables

Table 1. Thickness changes between the northern and the southern flank of the Jbel Amsittene Anticline for formations J-C and C1.

Table 2. Decrease in amount of shortening to the east, measured as unfolded line-length.

References

Amrhar, M., 1995. Évolution structurale du Haut Atlas occidental dans le cadre de l'ouverture de l'Atlantique centrale et de la collision Afrique--Europe: Structure, instabilités tectoniques et magmatisme. Thèse Doct. Etat, Univ. Cadi Ayyad, Marrakech.

Barnett-Moore, N., Hassan, R., Müller, R.D., Williams, S.E., Flament, N., 2017. Dynamic topography and eustasy controlled the paleogeographic evolution of northern Africa since the mid-Cretaceous: Dynamics topography in northern Africa. Tectonics 36, 929–944.

Benvenuti, M., Moratti, G., Algouti, A., 2017. Stratigraphic and structural revision of the Upper Mesozoic succession of the Dadès valley, eastern Ouarzazate Basin (Morocco). Journal of African Earth Sciences 135, 54–71.

Bertotti, G., Gouiza, M., 2012. Post-rift vertical movements and horizontal deformations in the eastern margin of the Central Atlantic: Middle Jurassic to Early Cretaceous evolution of Morocco. International Journal of Earth Sciences 101, 2151–2165.

Bonow, J.M., Japsen, P., Green, P.F., Cobbold, P.R., Pedreira, A.J., Lilletveit, R., Chiossi, D., 2009. Post-rift landscape development of north-east Brazil. Geological Survey of Denmark and Greenland Bulletin 17, 81–84.

Brautigam, K., Fernández-Blanco, D., Klaver, J.M., 2009. Late Jurassic–Early Cretaceous horizontal tectonics drives the Jbel Amsittene Anticline in the Haha Basin, Morocco. Master of Science Thesis. Vrije Universiteit Amsterdam.

Charton, R., Bertotti, G., Arantegui, A., Bulot, L., 2018. The Sidi Ifni transect across the rifted margin of Morocco (Central Atlantic): Vertical movements constrained by low-temperature thermochronology. Journal of African Earth Sciences 141, 22–32.

Charton, R.J.G., 2018. Phanerozoic Vertical Movements in Morocco. Delft University of Technology. https://doi.org/10.4233/UUID:FDA35870-18D9-4CA3-9443-199A1DCB0250

Choubert, G., and Union Internationale Pour L'étude du Quaternaire, 1965. Evolution de la connaissance du Quaternaire au Maroc. Service Géologique du Maroc.

Duffaud, F., Brun, L., Plauchut, B., 1966. Le bassin du Sud-Ouest marocain. Bassins Sédimentaires Du Littoral Africain. Publ. Assoc. Serv. Géol. Afric 1, 5–26.

Duval-Arnould, A., 2019. Controls on stratigraphic development of shelf margin carbonates: Jurassic Atlantic margin - Essaouira-Agadir Basin, Western Morocco. Doctoral Thesis. Manchester University.

Ellero, A., Malusà, M.G., Ottria, G., Ouanaimi, H., Froitzheim, N., 2020. Transpressional structuring of the High Atlas belt, Morocco. Journal of Structural Geology 135, 104021.

Ellouz, N., Patriat, M., Gaulier, J.-M., Bouatmani, R., Sabounji, S., 2003. From rifting to Alpine inversion: Mesozoic and Cenozoic subsidence history of some Moroccan basins. Sedimentary Geology 156, 185–212.

Frizon de Lamotte, D., 2005. About the Cenozoic inversion of the Atlas domain in North Africa. Comptes Rendus: Geoscience 337, 475–476.

Frizon de Lamotte, D., Andrieux, J., Guezou, J.C., 1991. Cinematique des chevauchements neogenes dans l'Arc betico-rifain; discussion sur les modeles geodynamiques. Bulletin de La Societe Geologique de France 162, 611–626.

Frizon de Lamotte, D., Saint Bezar, B., Bracène, R., Mercier, E., 2000. The two main steps of the Atlas building and geodynamics of the western Mediterranean. Tectonics 19, 740–761.

Frizon de Lamotte, D., Zizi, M., Missenard, Y., Hafid, M., El-Azzouzi, M., Maury, R.C., Charrière, A., Taki, Z., Benammi, M., Michard, A., 2008. The Atlas System. In: Michard, A., Saddiqi, O., Chalouan, A., de Lamotte, D.F. (Eds.), Continental Evolution: The Geology of Morocco, Lecture Notes in Earth Sciences. Springer Nature, Berlin Heidelberg, 133–202.

Ghorbal, B., 2009. Mesozoic to Quaternary thermo-tectonic evolution of Morocco (NW Africa). Vrije

Universiteit Amsterdam.
Ghorbal, B., Bertotti, G., Foeken, J., Andriessen, P., 2008. Unexpected Jurassic to Neogene vertical movements in “stable” parts of NW Africa revealed by low temperature geochronology. Terra Nova 20, 355–363.
Giles, K.A., Lawton, T.F., 2002. Halokinetic Sequence Stratigraphy Adjacent to the El Papalote Diapir, Northeastern Mexico. AAPG Bulletin 86, 823–840.
Gouiza, M., 2011. Mesozoic Source-to-Sink Systems in NW Africa:: Geology of vertical movements during the birth and growth of the Moroccan rifted margin. Vrije Universiteit Amsterdam.
Gouiza, M., Bertotti, G., Charton, R., Haimoudane, K., Dunkl, I., Anczkiewicz, A.A., 2019. New Evidence of “Anomalous” Vertical Movements along the Hinterland of the Atlantic NW African Margin. Journal of Geophysical Research, [Solid Earth]. https://doi.org/10.1029/2019JB017914
Gouiza, M., Charton, R., Bertotti, G., Andriessen, P., Storms, J.E.A., 2017. Post-Variscan evolution of the Anti-Atlas belt of Morocco constrained from low-temperature geochronology. International Journal of Earth Sciences 106, 593–616.
Green, P.F., Japsen, P., Chalmers, J.A., Bonow, J.M., Duddy, I.R., 2018. Post-breakup burial and exhumation of passive continental margins: Seven propositions to inform geodynamic models. Gondwana Research 53, 58–81.
Guiraud, R., Maurin, J.-C., 1992. Early Cretaceous rifts of Western and Central Africa: an overview. Tectonophysics 213, 153–168.
Hafid, M., 2006. Styles structuraux du Haut Atlas de Cap Tafelney et de la partie septentrionale du Haut Atlas occidental: tectonique salifère et relation entre l’Atlas et l’Atlantique. Notes Mém. Serv. Géol. Maroc 465, 172.
Hafid, M., 2000. Triassic–early Liassic extensional systems and their Tertiary inversion, Essaouira Basin (Morocco). Marine and Petroleum Geology 17, 409–429.
Hafid, M., Zizi, M., Bally, A.W., Ait Salem, A., 2006. Structural styles of the western onshore and offshore termination of the High Atlas, Morocco. Comptes Rendus: Geoscience 338, 50–64.
Hoggard, M.J., White, N., Al-Attar, D., 2016. Global dynamic topography observations reveal limited influence of large-scale mantle flow. Nature Geoscience 9, 456.
Jaïdi, S., Bencheqroun, A., Diouri, M., 1970. Carte Géologique du Maroc 1:100 000, Feuille Tamanar. Not. Mém. Serv. Géol. Maroc 201.
Japsen, P., Bonow, J.M., Green, P.F., Chalmers, J.A., Lidmar-Bergström, K., 2009. Formation, uplift and dissection of planation surfaces at passive continental margins – a new approach. Earth Surface Processes and Landforms 34, 683–699.
Japsen, P., Bonow, J.M., Green, P.F., Chalmers, J.A., Lidmar-Bergström, K., 2006. Elevated, passive continental margins: Long-term highs or Neogene uplifts? New evidence from West Greenland. Earth and Planetary Science Letters 248, 330–339.
Japsen, P., Chalmers, J.A., 2000. Neogene uplift and tectonics around the North Atlantic: overview. Global and Planetary Change 24, 165–173.
Japsen, P., Chalmers, J.A., Green, P.F., Bonow, J.M., 2012. Elevated, passive continental margins: Not rift shoulders, but expressions of episodic, post-rift burial and exhumation. Global and Planetary Change 90-91, 73–86.
Klitgord, K.D., Schouten, H., 1986. Plate kinematics of the central Atlantic. The Geology of North America 1000, 351–378.
Knott, S.D., Burchell, M.T., Jolley, E.J., Fraser, A.J., 1993. Mesozoic to Cenozoic plate reconstructions of the North Atlantic and hydrocarbon plays of the Atlantic margins. Petroleum Geology of Northwest Europe: Proceedings of the 4th Conference. Geological Society of London, 953–974.
Lanari, R., Faccenna, C., Fellin, M.G., Essaifi, A., Nahid, A., Medina, F., Youbi, N., 2020a. Tectonic Evolution of the Western High Atlas of Morocco: Oblique Convergence, Reactivation, and Transpression. Tectonics 39, 1459.
Lanari, R., Fellin, M.G., Faccenna, C., Balestrieri, M.L., Pazzaglia, F.J., Youbi, N., Maden, C., 2020b. Exhumation and Surface Evolution of the Western High Atlas and Surrounding Regions as

Constrained by Low-Temperature Thermochronology. Tectonics 39, 197.
Laville, E., Piqué, A., 1992. Jurassic penetrative deformation and Cenozoic uplift in the Central High Atlas (Morocco): A tectonic model. structural and orogenic inversions. Geologische Rundschau: Zeitschrift Fur Allgemeine Geologie 81, 157–170.
Laville, E., Pique, A., Amrhar, M., Charroud, M., 2004. A restatement of the Mesozoic Atlasic Rifting (Morocco). Journal of African Earth Sciences 38, 145–153.
Leprêtre, R., Missenard, Y., Barbarand, J., Gautheron, C., Saddiqi, O., Pinna-Jamme, R., 2015a. Postrift history of the eastern central Atlantic passive margin: Insights from the Saharan region of South Morocco. Journal of Geophysical Research, [Solid Earth] 120, 2014JB011549.
Leprêtre, R., Missenard, Y., Saint-Bezar, B., Barbarand, J., Delpech, G., Yans, J., Dekoninck, A., Saddiqi, O., 2015b. The three main steps of the Marrakech High Atlas building in Morocco: Structural evidences from the southern foreland, Imini area. Journal of African Earth Sciences 109, 177–194.
Le Roy, P., Piqué, A., 2001. Triassic–Liassic Western Moroccan synrift basins in relation to the Central Atlantic opening. Marine Geology 172, 359–381.
Luber, T.L., Bulot, L.G., Redfern, J., Nahim, M., Jeremiah, J., Simmons, M., Bodin, S., Frau, C., Bidgood, M., Masrour, M., 2019. A revised chronostratigraphic framework for the Aptian of the Essaouira-Agadir Basin, a candidate type section for the NW African Atlantic Margin. Cretaceous Research 93, 292–317.
Malusà, M.G., Polino, R., Feroni, A.C., Ellero, A., Ottria, G., Baidder, L., Musumeci, G., 2007. Post-Variscan tectonics in eastern Anti-Atlas (Morocco). Terra Nova 19, 481–489.
Medina, F., 1995. Syn- and postrift evolution of the El Jadida – Agadir basin (Morocco): constraints for the rifting models of the central Atlantic. Canadian Journal of Earth Sciences 32, 1273–1291.
Michard, A., Saddiqi, O., Chalouan, A., de Lamotte, D.F., 2008. Continental Evolution: The Geology of Morocco: Structure, Stratigraphy, and Tectonics of the Africa-Atlantic-Mediterranean Triple Junction. Springer.
Moragas, M., Vergés, J., Saura, E., Martín-Martín, J.-D., Messager, G., Merino-Tomé, Ó., Suárez-Ruiz, I., Razin, P., Grélaud, C., Malaval, M., Others, 2018. Jurassic rifting to post-rift subsidence analysis in the Central High Atlas and its relation to salt diapirism. Basin Research 30, 336–362.
Morley, C.K., Crevello, P., Ahmad, Z.H., 1998. Shale tectonics and deformation associated with active diapirism: the Jerudong Anticline, Brunei Darussalam. Journal of the Geological Society 155, 475–490.
Müller, R.D., Hassan, R., Gurnis, M., Flament, N., Williams, S.E., 2018. Dynamic topography of passive continental margins and their hinterlands since the Cretaceous., Gondwana Research. https://doi.org/10.1016/j.gr.2017.04.028
Neumaier, M., Back, S., Littke, R., Kukla, P.A., Schnabel, M., Reichert, C., 2016. Late Cretaceous to Cenozoic geodynamic evolution of the Atlantic margin offshore Essaouira (Morocco). Basin Research 28, 712–730.
Ouajhain, B., Daoudi, L., Laduron, D., Rocha, F., Jean, N., 2011. Jurassic clay mineral sedimentation control factors in the Essaouira Basin (Western High Atlas, Morocco). Geologica Belgica.
Oukassou, M., Saddiqi, O., Barbarand, J., Sebti, S., Baidder, L., Michard, A., 2013. Post-Variscan exhumation of the Central Anti-Atlas (Morocco) constrained by zircon and apatite fission-track thermochronology. Terra Nova 25, 151–159.
Peulvast, J.-P., Claudino Sales, V., Bétard, F., Gunnell, Y., 2008. Low post-Cenomanian denudation depths across the Brazilian Northeast: Implications for long-term landscape evolution at a transform continental margin. Global and Planetary Change 62, 39–60.
Pichel, L.M., Finch, E., Gawthorpe, R.L., 2019a. The Impact of Pre-Salt Rift Topography on Salt Tectonics: A Discrete-Element Modeling Approach., Tectonics. https://doi.org/10.1029/2018tc005174
Pichel, L.M., Huuse, M., Redfern, J., Finch, E., 2019b. The influence of base-salt relief, rift topography and regional events on salt tectonics offshore Morocco. Marine and Petroleum Geology 103, 87–113.

Piqué, A., Le Roy, P., Amrhar, M., 1998. Transtensive synsedimentary tectonics associated with ocean opening: the Essaouira–Agadir segment of the Moroccan Atlantic margin. Journal of the Geological Society 155, 913–928.
Piqué, A., Tricart, P., Guiraud, R., Laville, E., Bouaziz, S., Amrhar, M., Ouali, R.A., 2002. The Mesozoic-Cenozoic Atlas belt (North Africa): an overview. Geodinamica Acta 15, 185–208.
Poprawski, Y., Basile, C., Agirrezabala, L.M., Jaillard, E., Gaudin, M., Jacquin, T., 2014. Sedimentary and structural record of the Albian growth of the Bakio salt diapir (the Basque Country, northern Spain). Basin Research 26, 746–766.
Ruiz, G., Sebti, S., Negro, F., Saddiqi, O., Frizon de Lamotte, D., Stockli, D., Foeken, J., Stuart, F., Barbarand, J., Schaer, J.-P., 2011. From central Atlantic continental rift to Neogene uplift--western Anti-Atlas (Morocco). Terra Nova 23, 35–41.
Saddiqi, O., El Haimer, F.-Z., Michard, A., Barbarand, J., Ruiz, G.M.H., Mansour, E.M., Leturmy, P., Frizon de Lamotte, D., 2009. Apatite fission-track analyses on basement granites from south-western Meseta, Morocco: Paleogeographic implications and interpretation of AFT age discrepancies. Tectonophysics 475, 29–37.
Sahabi, M., Aslanian, D., Olivet, J.-L., 2004. Un nouveau point de départ pour l'histoire de l'Atlantique central. Comptes Rendus: Geoscience 336, 1041–1052.
Saura, E., Vergés, J., Martín-Martín, J.D., Messager, G., Moragas, M., Razin, P., Grélaud, C., Joussiaume, R., Malaval, M., Homke, S., Hunt, D.W., 2013. Syn- to post-rift diapirism and minibasins of the Central High Atlas (Morocco): the changing face of a mountain belt. Journal of the Geological Society 171, 97–105.
Scotese, C., 2016. PALEOMAP: Paleoatlas for GPlates and the paleodataplotter program. https://doi.org/10.1130/abs/2016nc-275387
Seguret, M., 1972. Étude tectonique des nappes et séries décollées de la partie centrale des Pyrénées. Thesis. Science Univ. Montpellier.
Sehrt, M., 2014. Variscan to Neogene long-term landscape evolution at the Moroccan passive continental margin (Tarfaya Basin and western Anti-Atlas). Heidelberg. https://doi.org/10.11588/heidok.00017463
Snedden, J.W., Liu, C., 2010. A compilation of Phanerozoic sea-level change, coastal onlaps and recommended sequence designations. Search and Discovery Article 40594, 3.
Stets, J., 1992. Mid-Jurassic events in the Western High Atlas (Morocco). Geologische Rundschau: Zeitschrift Fur Allgemeine Geologie 81, 69–84.
Tari, G., Molnar, J., Ashton, P., 2003. Examples of salt tectonics from West Africa: a comparative approach. Geological Society, London, Special Publications 207, 85–104.
Teixell, A., Arboleya, M.-L., Julivert, M., Charroud, M., 2003. Tectonic shortening and topography in the central High Atlas (Morocco). Tectonics 22, 1051.
Torsvik, T.H., Rousse, S., Labails, C., Smethurst, M.A., 2009. A new scheme for the opening of the South Atlantic Ocean and the dissection of an Aptian salt basin. Geophysical Journal International 177, 1315–1333.
Tucholke, B.E., Sawyer, D.S., Sibuet, J.-C., 2007. Breakup of the Newfoundland–Iberia rift. Geological Society, London, Special Publications 282, 9–46.
Westaway, R., Aït Hssaine, A., Demir, T., Beck, A., 2009. Field reconnaissance of the Anti-Atlas coastline, Morocco: Fluvial and marine evidence for Late Cenozoic uplift. Global and Planetary Change 68, 297–310.
Wilmsen, M., Neuweiler, F., 2007. Biosedimentology of the Early Jurassic post-extinction carbonate depositional system, central High Atlas rift basin, Morocco: Early Jurassic biosedimentology. Sedimentology 55, 773–807.
Zühlke, R., Bouaouda, M.-S., Ouajhain, B., Bechstädt, T., Leinfelder, R., 2004. Quantitative Meso-/Cenozoic development of the eastern Central Atlantic continental shelf, western High Atlas, Morocco. Marine and Petroleum Geology 21, 225–276.

INPUT FIELD DIP DATA TABLE

Jbel Amsittene Projection; UTM WGS 84; Zone 29

X	Y	Z	Measurement		Quality
[m]	[m]	[m]	DD1 [°]	Dip1 [°]	[A/B/C]
435800	3450762	361	11	60	B
435846	3450705	356	348	86	B
435908	3450662	357	170	51	A
435874	3450272	389	167	70	A
435961	3450252	397	162	72	B
435885	3450070	401	178	65	A
435997	3449959	409	179	60	B
436116	3449869	424	168	43	A
436309	3449617	452	341	40	B
436349	3449485	470	13	57	A
436639	3448875	625	350	18	B
436497	3449275	545	166	52	B
440038	3444268	337	324	23	B
440010	3444633	360	335	10	B
439612	3445486	345	0	0	B
439626	3445558	352	78	47	B
439678	3445778	397	162	65	B
439692	3445879	420	184	39	B
439777	3446146	470	158	42	B
439957	3446568	460	190	88	C
440007	3446874	522	165	54	A
440052	3447282	600	175	40	B
440063	3447567	632	180	45	A
440007	3446157	364	170	10	A
439931	3445773	345	188	18	A
439831	3445474	308	154	30	A
440239	3452440	449	334	80	B
440374	3451802	470	332	80	B
440285	3451615	522	330	78	A
440268	3451426	588	344	70	A
440283	3451224	665	345	55	B
440335	3451040	700	338	25	B
440346	3450851	733	2	45	A
440332	3450708	739	30	59	B
440493	3449913	770	50	52	B
440519	3449719	820	345	41	A
440400	3449475	815	332	80	C
440475	3449277	908	189	19	A
440585	3449522	881	152	26	B
440391	3450591	728	96	38	A
440380	3451459	537	336	61	A
436863	3451072		157	39	A
446620	3447724	448	286	20	A
446455	3447776	426	188	20	B
446362	448087	494	164	50	A
446774	447781	446	156	29	A
432490	448799	350	336	22	B
432455	3447959	393	311	62	A
432461	3447449	415	311	24	B
432595	3446120	452	166	42	A
432657	3445897	439	174	58	A

432613	3445378	421	356	68	A
433150	3444534	335	144	19	A
432589	3445344	421	358	68	A
435862	3450767	356	8	68	B
435855	3450693	362	2	89	A
436025	3450687	383	156	77	B
435952	3450684	375	158	64	A
435879	3450277	376	174	76	A
436106	3449892	416	188	60	B
436194	3449693	436	197	90	A
446419	3447674	427	168	30	A
433049	3444567	341	260	4	A
432986	3444655	357	160	29	A
432951	3444806	364	160	58	A
432914	3444933	378	179	37	A
432886	3444975	376	194	27	A
432862	3445170	350	156	52	A
432534	3445620	426	340	64	A
432546	3445764	426	170	85	A
435793	3450875	366	358	52	A
435885	3450995	358	158	86	A
435950	3451095	341	332	88	A
435824	3451849	482	334	18	A
436535	3451619	436	344	18	A
436588	3451578	419	120	49	B
436580	3451329	356	344	46	A
436477	3451153	338	348	86	A
436953	3450517	510	344	62	A
436992	3450260	581	342	28	A
437020	3449887	680	356	37	A
437010	3449702	703	349	28	A
437032	3449637	682	0	34	A
437048	3449539	622	270	27	B
437178	3449300	620	358	50	A
437370	3448970	719	356	40	A
437384	3448924	732	0	56	C
437403	3448810	777	154	41	C
437403	3448729	803	194	40	A
437434	3448518	867	352	40	B
437431	3448352	912	208	22	A
437334	3448286	879	294	10	B
437329	3448251	878	180	25	A
437273	3448144	873	114	34	A
437112	3448112	873	160	20	A
436783	3447975	863	200	20	A
436724	3447929	857	102	13	A
436789	3447882	855	124	22	A
436820	3447744	814	181	23	A
436802	3447717	797	164	30	A
436813	3447687	780	122	25	A
436722	3447634	725	183	35	A
436722	3447599	709	122	43	A
436728	3447539	689	224	46	A
436732	3447510	683	190	28	A
436741	3447467	669	124	28	B
436750	3447362	641	174	35	A

436754	3447276	625	131	46	A
436728	3447220	608	158	42	A
436703	3447145	575	167	47	A
436660	3447076	551	168	44	A
436679	3446956	541	166	42	A
436659	3446907	529	166	45	A
436641	3446755	512	166	46	A
436637	3446610	487	166	50	A
436589	3446482	441	168	55	A
436569	3446440	428	164	50	A
436551	3446352	418	171	42	A
436560	3446200	399	162	64	A
436631	3446084	386	156	42	A
436752	3445689	362	167	40	A
436698	3445510	353	138	41	A
440516	3449081	849	168	30	A
439729	3448909	882	140	14	B
439894	3448842	874	141	35	B
439956	3448724	852	135	28	B
439989	3448605	827	165	30	A
440004	3448522	835	180	28	B
439994	3448436	829	292	77	C
440000	3448191	782	140	28	B
440007	3448110	769	170	40	A
440136	3449132	757	220	26	A
440735	3449287	857	168	16	A
440890	3449178	856	180	31	A
441012	3449119	858	188	24	A
441189	3449200	846	141	16	A
433777	3444373	296	144	24	A
434093	3443830	276	64	16	B
433622	3444484	303	164	34	A
432410	3446184	450	170	60	B
432536	3446370	458	0	10	B
432658	3446811	433	325	88	B
432631	3446829	433	132	30	B
432098	3449379	337	0	12	B
432493	3447546	392	298	66	B
432506	3447586	404	291	74	B
432553	3447590	400	273	82	A
432574	3447558	403	277	60	B
432603	3447487	418	264	45	B
432631	3447434	444	230	18	B
432819	3447391	442	272	14	B
432850	3447347	440	249	40	B
432891	3447254	442	168	22	B
432975	3447198	439	154	25	A
433015	3447196	425	177	32	A
433020	3447229	428	184	20	B
433073	3447269	420	172	40	B
433184	3447298	430	184	37	A
433238	3447376	422	156	44	A
433318	3447449	427	168	43	A
433344	3447558	424	170	32	A
433371	3447627	435	155	22	A
433457	3447812	445	63	11	B

433508	3447798	451	146	24	B
433475	3447740	456	175	23	B
433437	3447811	446	98	9	A
433493	3447909	457	116	21	B
433453	3447965	449	70	27	A
433417	3448032	448	76	23	A
433413	3448080	429	350	35	B
433395	3448078	424	32	30	B
433467	3448067	442	73	20	B
433453	3448076	443	14	13	A
433304	3448092	442	4	27	B
433248	3448130	428	349	31	B
433161	3448128	409	336	58	A
433062	3448129	422	333	60	B
432980	3448111	424	332	18	B
432808	3447994	407	308	67	B
432755	3447963	405	312	77	B
432673	3447843	396	277	60	B
432640	3447801	397	301	58	B
432649	3447679	385	261	85	A
432690	3447582	383	231	54	B
432782	3447518	405	207	52	C
432839	3447492	392	184	51	B
432923	3447519	384	181	31	A
432960	3447593	387	151	52	A
433140	3448036	398	350	71	B
432604	3447696	378	305	89	B
432553	3447709	387	303	47	A
432491	3447823	395	328	19	B
432516	3447896	389	144	85	A
432516	3447753	372	292	88	B
432437	3447630	417	179	30	B
446436	3451853	603	35	27	B
446380	3451799	556	56	15	A
446198	3451618	572	48	28	A
446120	3451517	592	77	22	A
446030	3451476	601	85	30	B
445896	3451414	610	72	24	A
445767	3451346	635	49	18	A
445566	3451270	675	75	20	A
445409	3451235	698	62	23	A
445249	3451207	718	70	22	B
445120	3451173	739	64	16	A
444979	3451107	770	97	20	B
444799	3450983	806	53	17	B
444718	3450975	810	68	8	B
444480	3451024	817	59	12	B
444394	3451005	826	64	11	C
443624	3450569	876	124	14	B
443609	3450422	870	108	7	B
443106	3450449	877	127	13	B
442846	3450447	883	90	15	A
442442	3450108	866	140	14	B
442057	3449873	852	266	15	B
441862	3449728	844	292	9	B
441570	3449611	860	330	8	B

441378	3449531	844	240	7	A
444537	3450205	805	147	5	B
444649	3450172	796	136	20	A
444712	3450425	780	134	12	B
444985	3450538	726	120	16	B
445292	3450537	731	104	10	B
445511	3450808	712	49	9	B
445393	3450888	704	104	20	A
445319	3451121	690	56	10	A
445462	3451388	660	37	21	B
445175	3451770	640	50	22	B
445402	3451720	596	50	18	A
445697	3451742	581	48	22	A
445976	3451595	575	45	14	A
448710	3449930	484	210	29	C
448823	3449959	484	12	31	A
449136	3449718	481	185	26	B
449243	3449745	498	65	20	A
449296	3449775	483	34	20	A
449081	3449932	507	233	2	B
449141	3449949	538	222	22	B
449263	3450027	534	210	24	B
449312	3450042	517	216	22	A
449344	3450108	518	159	20	A
449355	3450215	558	275	10	B
449395	3450436	575	180	24	C
449393	3450657	568	131	10	C
449344	3450336	574	148	24	B
448878	3451171	456	163	40	B
448842	3451160	499	349	18	A
448612	3451300	494	359	18	A
448680	3451460	500	26	18	B
448760	3451561	506	350	17	A
448835	3451484	504	273	15	A
448972	3451463	505	158	40	A
449110	3451456	503	34	9	B
449071	3451534	502	318	20	C
449045	3451587	506	349	47	A
448524	3451031	478	322	17	A
448481	3451004	496	120	42	B
448451	3450450	476	80	18	A
448243	3451528	502	341	29	B
421555	3440864	58	180	57	A
421571	3440993	74	196	88	B
421618	3441131	98	182	64	A
421611	3441208	123	185	42	A
421672	3441352	157	186	48	A
421667	3441402	166	180	22	A
421667	3441504	193	138	5	B
421714	3441951	215	190	3	B
421675	3442064	220	38	32	B
421684	3442209	216	16	7	B
421760	3442691	220	324	15	B
421831	3443084	221	299	27	B
421863	3443170	215	268	12	A
421881	3443251	211	344	11	B

421783	3443811	215	320	24	B
421690	3444007	205	278	14	A
420782	3443738	136	298	32	B
421018	3443723	171	108	8	B
421129	3443716	174	282	12	B
421216	3443697	194	278	14	A
421554	3443503	192	278	17	A
421587	3443424	177	266	12	A
421663	3443317	189	310	15	B
432451	3447894	400	308	58	B
432476	3448052	399	320	80	B
432542	3448282	369	154	84	B
432591	3448237	379	132	89	B
432582	3448096	383	124	89	B
432557	3448071	382	149	57	B
432544	3447934	374	135	50	B
432503	3447999	364	318	56	A
432496	3448073	370	307	60	A
432531	3448183	367	158	88	B
439970	3452800	420	343	39	B
439907	3452955	432	352	24	B
439788	3453318	554	346	20	B
439738	3453401	600	346	25	B
439863	3453247	500	12	14	B
439947	3453132	453	356	16	B
439532	3452487	413	318	24	A
439545	3452351	398	339	28	A
439520	3452266	393	335	68	A
439485	3452216	399	336	78	A
439492	3452116	411	333	82	B
438735	3444323	316	189	30	B
438439	3444330	343	150	21	A
438207	3444252	344	148	20	B
437843	3443692	274	156	14	C
445432	3446770	431	168	19	A
445200	3447036	415	177	33	B
449017	3447275	548	310	15	B
448511	3448960	481	140	20	B
448388	3449185	487	164	10	A
445087	3447400	501	5	28	B
444992	3447439	536	346	24	C
444962	3447457	541	150	31	B
444858	3447635	554	124	44	B
444747	3447635	536	154	57	A
444953	3448310	587	140	20	B
445019	3448408	587	196	26	B
445020	3448699	584	146	34	A
445047	3448845	619	162	30	B
445052	3449003	635	136	25	B
445009	3449237	664	142	28	B
444830	3449393	648	143	21	A
444659	3449648	689	143	20	A
444625	3449724	699	137	22	B
444601	3449252	586	162	23	A
444862	3448883	550	148	25	A
444838	3448577	532	168	28	B

444781	3448427	526	191	23	A
444761	3448155	503	168	16	A
444736	3447380	513	172	15	A
444678	3447306	505	146	36	B
443718	3453029	488	189	50	B
443768	3452517	537	357	65	B
443755	3452404	520	348	46	A
443731	3452348	543	333	60	A
443736	3452246	574	16	25	A
443715	3452191	612	358	48	A
443682	3452050	655	357	37	B
443675	3451973	671	2	21	A
443635	3451842	707	21	20	B
443778	3451594	732	5	16	B
443775	3451496	751	48	10	A
443852	3451325	790	47	11	B
443918	3451233	824	75	7	B
446954	3447898	455	15	30	B
447007	3447913	442	250	27	B
447153	3447928	448	350	50	B
447335	3447896	457	1	31	B
447420	3447825	457	96	18	B
447592	3447671	461	167	12	B
447685	3447635	467	205	20	B
447777	3447682	471	310	22	A
447960	3447766	474	76	5	A
448016	3447794	481	64	22	A

INPUT FIELD DIP DATA TABLE

Jbel Amsittene **Projection; UTM WGS 84; Zone 29**

Outcrop #	Figure	X	Y	Z	Lithology	Comment
#	#	[m]	[m]	[m]	[-]	[-]
Oc1_W-E	Fig. 3B	433150	3444534	335	Limestone	Gently tilted bedding with conjugate sets
Oc2a_N-S	Fig. 3C	432914	3444933	378	Limestone, marl and calcarenite	Strata cut by neptunian dyke oriented at present 272/83
Oc2b_N-S	Fig. 3C	432914	3444933	378	Limestone, marl and calcarenite	Strata cut by neptunian dyke oriented at present 272/83
Oc3_N-S	Fig. 3D	432914	3444975	376	Limestone	Folded and faulted soft sediments
Oc5a_S-N	Fig. 3f	432461	3447449	415	Limestone with marl intercalations	Folds and reverse faults
Oc5b_S-N	Fig. 3F	432461	3447449	415	Limestone with marl intercalations	Folds and reverse faults
Oc6_N-S	Fig. 4B	436374	3449046	502	Limestone	Fold
Oc7a_N-S	Fig. 4C	436116	3449869	424	Limestone grainstone	Underthrust in overturned strata, S0 is 175/73
Oc7b_N-S	Fig. 4C	436116	3449869	424	Limestone grainstone	Underthrust in overturned strata, S0 is 175/73
Oc8a_S-N	Fig. 5B	439931	3445773	345	Limestone	A high-angle reverse fault cuts thick bed and deforms soft sediments
Oc8b_S-N	Fig. 5B	439931	3445773	345	Limestone	A high-angle reverse fault cuts thick bed and deforms soft sediments
Oc9a_S-N	Fig. 5C	441189	3449200	846	Limestone	Calcite shear zone fractures
Oc9b_S-N	Fig. 5C	441189	3449200	846	Limestone	Calcite shear zone fractures
Oc10a_SW-N	Fig. 7	446451	3447776	426	Limestone	30-m long wedge pinching southwards with faulted underlaying strata
Oc10b_S-N	Fig. 7	446451	3447776	426	Limestone	30-m long wedge pinching southwards with faulted underlaying strata

Oc1_W-E

Oc2a_N-S

Oc2b_N-S

Oc3_N-S

Oc5a_S-N

Oc5b_S-N

Oc6_N-S

Oc7a_N-S

Oc7b_N-S

Oc8a_S-N

Oc8b_S-N

Oc9a_SW-NE

Oc9b_NE-SW

Oc10a_SW-NE

Oc10b_S-N